FLEXIBLE MICROMACHINED TEXTILE-LIKE GRAPHENE BIOELECTRODES FOR ELECTROCARDIOGRAPHY MONITORING

by
SEBA NUR ALHASAN

Submitted to the Graduate School of Engineering and Natural Sciences
in partial fulfillment of
the requirements for the degree of Master of Science

Sabanci University
July 2024

To my dear family and friends who are always by my side…

ABSTRACT

FLEXIBLE MICROMACHINED TEXTILE-LIKE GRAPHENE BIOELECTRODES FOR ELECTROCARDIOGRAPHY MONITORING

SEBA NUR ALHASAN

ELECTRONICS ENGINEERING MSc. THESIS, JULY 2024

Supervisor: Assoc. Prof. Murat Kaya YAPICI

Keywords: Biosensor, ECG Electrode, Flexible, Graphene Oxide, Vitamin C, Medical Garment, Nanomaterials, Personalized Medicine, Smart Fabric, Wearable Electronics

Dry electrodes capable of accurately recording vital signals represent a promising future for wearable long-term health monitoring devices. This thesis introduces an ultrathin, flexible, textile-like, microstructured dry electrode that features self-adhesive capabilities for conformal attachment to skin facilitating wearable electrocardiography (ECG) monitoring applications. The electrode design employs Poly (methyl methacrylate) (PMMA), a material commonly used in the textile industry, onto which functional graphene layers are coated along with photo-patternable SU-8 epoxy as the backing layer. The textile-like structure of the micromachined electrodes includes 100 µm gap sizes with 100 µm spacing, achieved by patterning PMMA through oxygen plasma and hard-mask layer without requiring expensive e-beam lithography (EBL) processes. Graphene oxide is applied to the electrodes via drop casting as the active material for signal acquisition, followed by a simple reduction step using eco-friendly pure vitamin C (L-ascorbic acid). The electrode's functionality for ECG monitoring is demonstrated by reporting the skin-contact impedance and benchmarking the electrodes against clinical-grade pre-gelled, “wet” Ag/AgCl electrodes, achieving a correlation of up to 98.84%. Additionally, the electrodes' capability to record biopotentials during physical activities with the presence of motion is demonstrated both in dry and wet conditions to verify their performance for wearable applications. The results demonstrate the remarkable self-adhesiveness, flexibility, reusability, and water resistance of the electrodes, maintaining conformal skin-electrode contact and offering high-quality signal acquisition.

ÖZET

ELEKTROKARDIYOGRAFI IZLEME IÇIN ESNEK MIKROMAKINE TEKSTIL-BENZERI GRAFEN BIYOELEKTROTLAR

SEBA NUR ALHASAN

ELEKTRONIK MÜHENDISLIĞI YÜKSEK LISANS TEZI, TEMMUZ 2024

Danışman: Assoc. Prof. Murat Kaya YAPICI

Anahtar Kelimeler: Biyosensör, EKG Elektrodu, Esnek, Grafen Oksit, C Vitamini, Tıbbi Giysi, Nanomalzemeler, Kişiselleştirilmiş Tıp, Akıllı Kumaş, Giyilebilir Elektronik

Hayati sinyalleri doğru bir şekilde kaydedebilen kuru elektrotlar, giyilebilir uzun süreli sağlık izleme cihazları için umut verici bir geleceği temsil etmektedir. Bu tez, giyilebilir elektrokardiyografi (EKG) izleme uygulamalarını kolaylaştıran cilde uyumlu bir şekilde tutturulabilmesi için kendinden yapışkanlı özelliklere sahip ultra ince, esnek, tekstil benzeri, mikro yapılı bir kuru elektrodu tanıtmaktadır. Elektrot tasarımında, tekstil endüstrisinde yaygın olarak kullanılan bir malzeme olan Poli (metil metakrilat) (PMMA) kullanılmış olup, bunun üzerine fonksiyonel grafen katmanları kaplanmış ve destek katmanı olarak foto-desenlenebilir SU-8 epoksi kullanılmıştır. Mikro-işlenmiş elektrotların tekstil benzeri yapısı, pahalı e-beam litografi (EBL) işlemleri gerektirmeden PMMA'nın oksijen plazması ve sert maske tabakası yoluyla desenlendirilmesiyle elde edilen 100 µm aralıklı 100 µm boşluk boyutları içerir. Grafen oksit, sinyal alımı için aktif malzeme olarak damla döküm yoluyla elektrotlara uygulanır ve ardından çevre dostu saf C vitamini (L-askorbik asit) kullanılarak basit bir indirgeme adımı gerçekleştirilir. Elektrotun EKG izleme işlevselliği, cilt temas empedansının raporlanması ve elektrotların klinik sınıf önceden jelleştirilmiş, "ıslak" Ag/AgCl elektrotlarla karşılaştırılmasıyla gösterilmiş ve %98,84'e varan bir korelasyon elde edilmiştir. Ayrıca, elektrotların giyilebilir uygulamalar için performanslarını doğrulamak amacıyla hareketin var olduğu fiziksel aktiviteler sırasında biyopotansiyelleri kaydetme kabiliyeti hem kuru hem de ıslak koşullarda gösterilmiştir. Sonuçlar, elektrotların dikkat çekici

kendinden yapışkanlığını, esnekliğini, yeniden kullanılabilirliğini ve suya dayanıklılığını, uyumlu cilt-elektrot temasını koruduğunu ve yüksek kaliteli sinyal alımı sunduğunu göstermektedir.

ACKNOWLEDGEMENTS

I would like to emphasize my sincere appreciation to my supervisor, Professor Murat Kaya Yapıcı, for imparting the best of his knowledge to me that enabled me to achieve my master's studies through his guidance and enduring support. His insightful patience, encouragement, and belief in me have been truly invaluable throughout this journey. I am deeply grateful for his mentorship, which has greatly enriched both my academic and personal growth. Also, I would like to thank my jury members for their precious time spent on my thesis.

I would like to extend my heartfelt thanks to my friends Sajjad Mirbakht and Saygun Güler, who helped me throughout this thesis along with their constant support and encouragement. Their companionship and assistance were crucial in overcoming the challenges I faced during this journey. I am deeply grateful to Osman Şahin and Rayan Bajwa for their invaluable guidance in teaching me the principles of working in a cleanroom environment. I also wish to thank Özberk Öztürk for his assistance in building the impedance circuit, and Gökmen Şanlı for his help with the FTIR experiment. Furthermore, I am thankful to my groupmates (SUMEMS) for their invaluable support and precious discussions, which significantly enriched my research and academic experience. Their insights and collaborative spirit fostered an environment of academic growth and friendship that I deeply appreciate. Additionally, I would like to express my gratitude to my dear friends Gülşen Zal, Zobia Batool, Rabia Mercimek, Serra Ersoy, and Ayça Aydurmuş for their support and the unforgettable memories they provided. They truly became my second family during my master's studies, and their presence made this journey much more enjoyable and fulfilling.

Finally, I have the deepest gratitude for my parents and siblings, who have always supported me in achieving my goals. I am especially thankful to my brother, Mohammed Alhasan, who believed in me even more than I believed in myself. His unwavering support, wise advice, patience, and exemplary guidance have been invaluable to me throughout this journey and my life. I will forever be grateful for their presence in my life, and their unwavering support means more to me than words can express.

TABLE OF CONTENTS

LIST OF TABLES

LIST OF FIGURES

LIST OF ABBREVIATIONS

CHAPTER 1.

INTRODUCTION

1.1 Dry Electrodes for Electrocardiography

Cardiovascular monitoring using electrocardiography (ECG) is a commonly used diagnostic technique with a vast application area in health informatics including identification of acute stress levels [1], emotion recognition [2], diagnosis of various cardiac disease including coronary syndromes and myocardial infarction [3, 4]; as well as, determining drug efficiency in treatment [5]. While short-term patient monitoring provides information for some of the aforementioned health issues, many require continuous and long-term tracking of biopotentials for an accurate diagnosis. A typical procedure for acquiring ECG data involves using Ag/AgCl electrodes with adhesive backing for reliable attachment to the skin. Although these wet electrodes have proved highly accurate, they have two fundamental issues: 1) conductive gels degrade over time affecting the signal quality, and 2) strong adhesives induce skin irritation and trauma [6]. Such limitations have led to the rapid growth of dry electrode alternatives which do not require skin preparation and viscous gels prior to use [7]. Eliminating the gel not only resolves skin irritation but also assures reusability over extended durations.

1.2 Motivation

In this thesis, we demonstrate a straightforward approach of utilizing O_2 plasma-based dry etching along with photolithography to selectively etch and structure the PMMA surface, much like a weft and warp pattern. This unique approach allowed us to "artificially-weave" the PMMA, and essentially realize a textile-like polymeric (TPM) surface. To render a mechanically robust TPM structure, a 50 μm-thick layer of SU-8 was used as the backing layer, which supported the relatively thin PMMA surface. Thereafter, the TPM surface could be functionalized by drop-casting graphene oxide (GO) and converting to reduced graphene oxide (rGO) using an environmentally-friendly vitamin C (L-ascorbic acid) reduction agent, effectively realizing flexible TPM electrodes for biosignal monitoring. We demonstrate the excellent performance of TPM electrodes in recording ECG signals alongside conventional Ag/AgCl electrode, where the TPM electrodes achieve a correlation score of 98.84%, while the SNR values are almost equal to those of the conventional electrodes. Alongside their performance in biopotential recording, we demonstrate the superior mechanical properties of this new artificially-weaved TPM electrode, together with its attributes such as electrode flexibility, self-adhesive properties, ability to continuously record signals up to tens of minutes and long-term stability even after immersion to water for 5 days.

CHAPTER 2.

TYPES OF DRY ELECTRODES

2.1 Microneedle Electrodes

Recently, various types of dry electrodes have been proposed including: microneedle type [8], capacitive [9], and surface electrodes [10]. Despite their potential side effects, including inflammation [11], various fabrication strategies were developed to realize microneedle electrodes in an effort to minimize or mitigate motion artifacts by penetrating the outer skin layer [12]. For instance, deep X-ray lithography and copper (Cu) electroplating were used to pattern grooves out of Poly (methyl methacrylate) (PMMA) for brain-computer interface applications [13]. SU-8 microneedle arrays were built for electroencephalogram (EEG) on a flexible polydimethylsiloxane (PDMS) mold with a porous parylene release layer preventing the metal from peeling off of the substrate [14]. Another study proposes a fabrication process where the laser-direct writing (LDW) was used to create pattern on a polyethylene terephthalate (PET) substrate, and the magnetorheological drawing lithography (MRDL) was used for constructing microneedles on top of it [15]. UV maskless lithography was also used with gold (Au) sputtering to construct conical microneedles for various biopotential measurements [16].

2.2 Capacitive Electrodes

Alternatively, to realize non-contact, capacitive ECG electrodes, aluminum conductive foil and copper were used and dry electrodes were formed on polyimide substrates [17]. Another approach relied on simply attaching conductive textiles on dry polymer foams to realize a cloth-attachable and capacitive biopotential sensing monitor [18]. Copper/nickel-plated composition was also used to develop a capacitive infant underwear design [19]. Likewise, a three-electrode ECG t-shirt model with built-in driven right leg electrode and two capacitive differential electrodes [20], and a manually adjustable, pressure-sensitive capacitive belt design were proposed [21]. Despite the steady progress and various efforts to adjust the skin-electrode contact pressure [22, 23], capacitive electrodes inherently suffer from motion artifacts and display high skin-electrode impedance due to the inevitable gap between the sensing region and the skin surface or clothing [24].

2.3 Surface Polymeric Electrodes

Surface polymeric electrodes are also great alternatives for biopotential measurements due to their intrinsic mechanical properties, such as stretchability and elasticity. Poly(3,4-ethylene dioxythiophene): polystyrene sulfonate (PEDOT: PSS) and PDMS are used mostly in skin-like electronics [25]. Applications also include waterborne polyurethane (WPU) for improved stretchability as well as D-sorbitol for better adhesiveness and tolerance to motion artifacts [26]. Along the same lines, tattoo electrodes were proposed where conductive polymers were formed on commercial decal paper using inkjet printing [27], and thin film metals were deposited on PET) substrate [28]. Carbon nanofillers were used to build micropillars to improve the attachment without penetrating skin [29], [30].

2.4 Graphene-Based Electrodes

To realize surface biopotential electrodes, carbon-based materials, and most recently graphene [31] has been widely preferred in biopotential measurement applications due to

its intrinsic properties, such as electrical conductivity [32], thermal conductivity [33], and durability [34]. Skin-compatible tattoos employing graphene were also developed [35] to increase the signal-to-noise ratio by excellent adhesion to the skin through self-adhesive materials [36] and Van der Waals forces [37].

2.5 Textile Electrodes

Of particular importance are textile electrodes as they are naturally wearable, soft, and feasible to implement not only in fashionable clothes [38]; but also, in accessories such as headphones [39]. Moreover, the mesh layout of the weaves in textiles make them suitable for biopotential measurements on the skin as this structure can route the signal energy in the "z" direction; normal to the skin surface. This allows easy and robust electrical interfacing to the textile electrodes and therefore a stable skin-electrode contact that is free from potential disturbance due to sideway interconnects (e.g. with FPC cables and connectors) is achieved. In an effort to unite the favorable properties of graphene and textiles, ordinary fabrics such as nylon, and cotton were functionalized by graphene through a straightforward dip-dry-reduce strategy and wearable, soft graphene textile biopotential electrodes with excellent performance were realized [31].

2.5.1 Microfabrication of PMMA

Among different materials used in synthesizing textile fibers such as polyester, nylon, cotton and acrylic fabrics; acrylic fabrics have a spin-coatable and patternable form which is Poly (methyl methacrylate) (PMMA). The very availability of a spin-coatable and patternable PMMA opens up new venues to realize “textile-like” Micro/nanostructured surfaces similar to weaved textiles which can be functionalized by dip-coating for instance. To pattern this material electron beam lithography (EBL) is widely used which can transfer the pattern with high-resolution pattern [40], yet EBL is a resource-intensive method requiring dedicated infrastructure and lengthy process cycles [41]. In contrast as

an alternative, dry etching using O_2 plasma is effective in removing PMMA [42], [43]. However, the O_2 plasma method requires the deposition of an additional resist layer (protection layer) on the PMMA to function as a mask, safeguarding specific areas of the underlying PMMA. Consequently, the O_2 plasma selectively etches the exposed regions.

CHAPTER 3.

BACKGROUND ON BIOPOTENTIAL ELECTRODES AND ELECTROCARDIOGRAPHY

3.1 Electrical Activity of Heart

The heart is considered to be a pump more than an organ, where the heart receives blood from venous blood vessels then ejects it to the atrial blood vessels. The heart consists of two muscular pumps, the right and left atrium, and two reservoirs, the right and left atrium [44].

The tissue of the heart consists of different types: nodal tissue, sinoatrial (SA) and atrioventricular (AV) tissue, atrial, Purkinje, and ventricular tissue. Each tissue type has its own electrically excitable cells, which exhibit an action potential specific to the tissue type. The SA node, also called the pacemaker, initiates each heartbeat. The impulse is then transmitted to the atria, activating first the right and then the left atrium. After passing the action potential through the atria, the pulse reaches the AV node located at the base of the right atrium. A delay occurs at the AV node, ensuring the complete contraction of the atria before the pulse continues its way to the His bundle and its branches—the right and left bundle branches. The right bundle branch extends to the right side of the interventricular septum to the apex of the right ventricle, while the left bundle crosses to the left side of the septum. These branches further extend to the Purkinje network, which runs within the ventricles. Generally, the impulses travel through these interconnections in a parallel manner, from the inside to the outside, resulting in a coordinated contraction of the ventricles to pump blood into the body [45]. Figure 1 illustrates the pathway of the cardiac action potential within the conduction system, along with the associated conduction velocities.

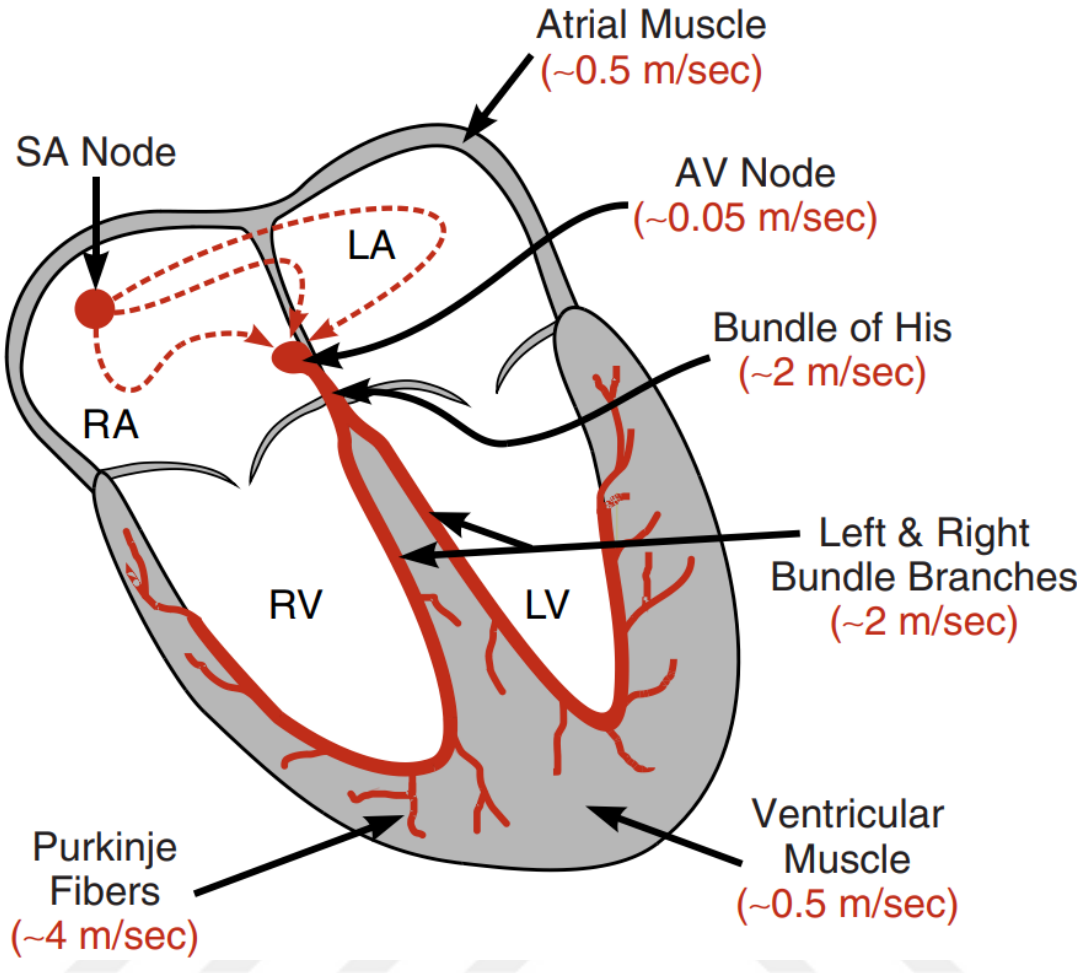

Figure 1 The conduction system of the heart [44].

The electrocardiogram (ECG) is a recording of the potential difference on the skin surface. This potential arises from the depolarization and repolarization of the heart muscle. Action potentials within the cardiac cells generate currents in the extracellular fluid. The currents generate small potential differences across the body surface around 1 mv which can vary. The magnitude of the skin potential difference relies on the size of the extracellular current. Which in turn depends on the mass of myocardium that is activated. Consequently, the surface ECG can detect the activity of atrial and ventricular muscle but fails to detect the pacemaker. The PR interval in the ECG waveform represents the taken time for the action potential to run across both atria then through the AV node and the bundle of His–Purkinje system into the ventricle. Most often the PR interval indicates the delay in transmission through the AV node, which allows atrial systole to complete before ventricular systole begins. The typical duration of the PR interval is around 0.2s. The QRS complex represents the depolarization of ventricular muscle, producing a large potential difference. Sometimes not all the components are

presented in the record, and the complex might consist of just RS or QR. The typical duration of the complex is less than 0.12 seconds. The ST segment, an extension of the QRS complex to the start of the T wave. The ST segment represents the ventricular depolarization and ejection. Due to the depolarization uniformity no extracellular current flows during the ST segment, rendering it isoelectric. Finally, T wave represents the Ventricular repolarization signifying the recovery of the ventricular. It is slower and less synchronous than depolarization, resulting in a lower magnitude than QRS complex [46]. Figure 2 demonstrates the cardiac action potential aligned with the ECG wave.

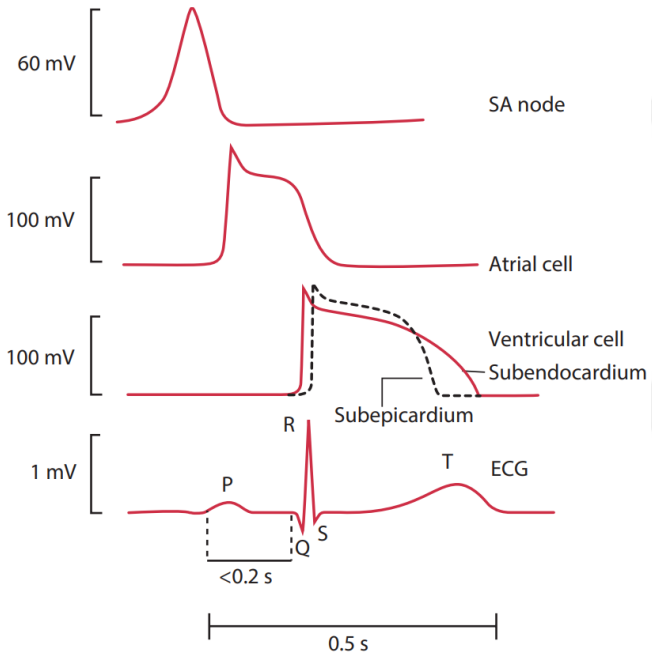

Figure 2 The cardiac action potential and ECG wave [46].

3.2 ECG Signal Measurement and Lead Points

The first electrocardiogram (ECG) was recorded in 1887 from with a mercury capillary. In 1901 Willem Einthoven successfully recorded ECG signal using string galvanometer, and established the famous triangle with leads I, II, and III which are called bipolar limb leads, using electrodes placed on both arm and left leg connected across a voltmeter to record the signal from the heart as shown in figure 3. In each lead there in a plus sign of

the edge of the tringle represent the positive terminal while two negative signs represent the negative terminals [47].

In lead I configuration the left arm is connected to the positive terminal and right arm is connected to the negative terminal which considered as the top of Einthoven's triangle with angle of zero. Thus, the positioned electrodes form a sensing triangle around the heart. In lead II, right arm is connected to the positive terminal and left arm is connected to the negative terminal, resulting in a view angle of the heart up to +60º. While in lead III left leg is connected to the positive terminal and left arm is connected to the negative terminal, resulting in heart view angle of +120º. Additionally, Clinical ECG signal usually taken using chest electrodes, which they are six electrodes V1, V2, V3, V4, V5 and V6, as shown in figure 3. These leads are connected to the positive terminal of voltermeter, and all three limb leads are connected to the negative terminal, thus they encircle the heart. There are three unipolar limb leads referred as augmented limb leads, aVL, aVR, aVF, demonstrating the heart angle of -30, -150, +90, respectively [46]. These leads are also mathematically related to Einthoven leads [48]. The equations of the aVL, aVR, and aVF are expressed as:

$$aVf = II - 1/2I \tag{3.1}$$

$$aVL = I - 1/2II \tag{3.2}$$

$$aVL = -(3/4\ I + 1/2\ aVF) \tag{3.3}$$

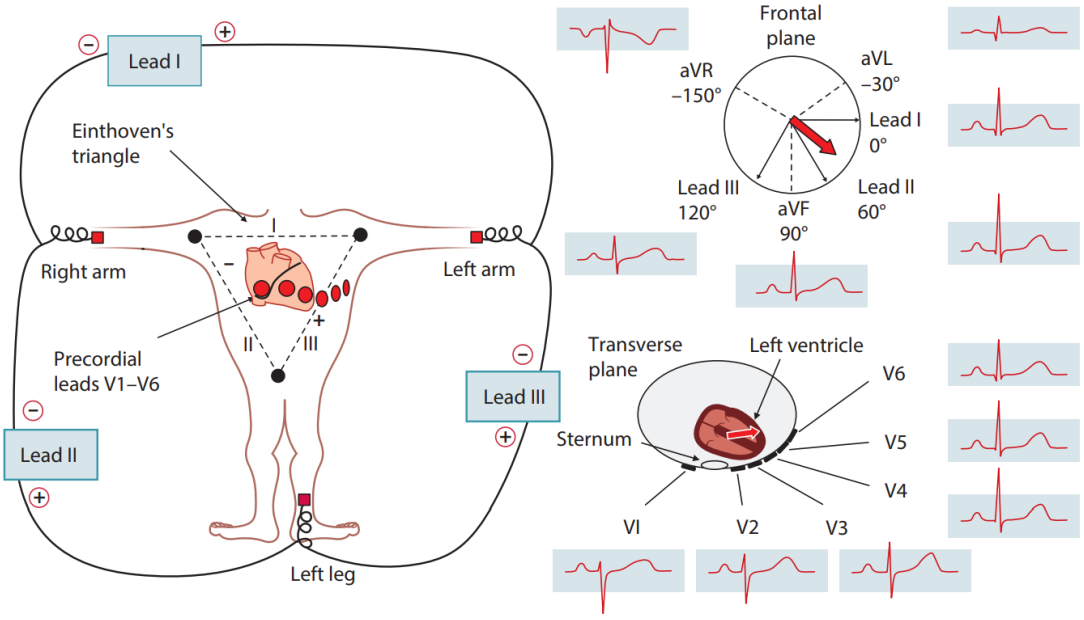

Figure 3 Electrode positions to record a 12-lead ECG [46].

CHAPTER 4.

MATERIALS AND METHODS

4.1 Fabrication of textile-like polymeric microstructure electrodes (TPM) electrodes

4.1.1 Deposition of SiO_2 sacrificial layer

The process begins with depositing sacrificial material with a thickness of 500 nm on a Si wafer by using plasma-enhanced chemical vapor deposition (PECVD) (Oxford Plasmalab System 100). Silane (SiH_4) and nitrous oxide (N_2O) gases were used in PECVD to grow the SiO_2 film. SiO_2 layer served as a sacrificial layer to be etched fully at the end of the fabrication process and release the structure.

4.1.2 Photo-patterning of SU-8 resist

A 50 μm thick SU-8 negative photoresist (Kayaku Advanced Materials, Westborough, MA, USA) with Young's modulus of 2 GPa was used as a backing and to provide mechanical stability, as PMMA alone is too thin. It was spin-coated at 3000 rpm for 30 s with an initial spread cycle of 10 seconds at 300 rpm, then soft-baked at 65°C for 5 min and 95 °C for 15 min, followed by exposure with 365 nm UV light at a dose of 70 mJ/cm^2 for 9 s. Next, post-exposure bake for 2 min at 65 and 7 min at 95°C, then 4 min development in SU-8 developer (i.e. 1-methoxy-2-propyl acetate), the microscope image of the SU-8 is shown in Figure 4a.

4.1.3 Photo-patterning of Cu hard mask for PMMA etching

PMMA (495K MW PMMA- C4) was spin-coated on the sample at 4000 rpm for 45 s to reach 400 nm thickness. It was later baked at 180 ºC for 10 minutes. Figure 4b shows the sample after coating the PMMA. 500 nm thick copper (Cu) was used as a protective layer which was thermally deposited (Nanovak R&D, Ankara, Turkey) on PMMA under 10^{-6} Torr chamber vacuum pressure (Figure 4c). AZ5214 photoresist (PR) was spin-coated at 4000 rpm for 30 s to reach 1.2 μm of thickness. The sample was then baked for 60 s at 105 ºC on a hot plate. After the second mask alignment, it was exposed with 365 nm UV light at a dose of 70 mJ/cm^2 followed by immersion in AZ-726 developer for 40 s. The sample was finally immersed in distilled water (DI water) and dried with pressurized N_2 gas. The Cu layer was utilized as a hard mask to protect the underlying PMMA during O_2 plasma exposure.

4.1.4 Etching PMMA layer

The substrate was immersed for 30 s in Cu etchant mixture of acetic acid, hydrogen peroxide solution, and DI water with a ratio of (1:1:18). Figure 4d demonstrates a microscope image of the sample after etching the copper inside the squares. Next, to pattern the PMMA, O_2 plasma etching (Oxford Plasmalab System 100) was applied for 13 minutes so that the PR and PMMA were removed from unprotected parts on Cu. Figure 4e demonstrates a microscope image of the sample after etching the PMMA inside the gaps.

4.1.5 Lift-off SU-8/PMMA

To finalize the fabrication, Cu layers were chemically etched again using acetic acid and hydrogen per oxide solution, Figure 4f demonstrates the microscope image of the sample after etching the top layer of copper. An array of four SU-8/PMMA electrodes before release is shown in Figure 5. The samples were kept in Buffered oxide etch BOE 7:1

(MicroChemicals GmbH, Ulm, Germany) solution for 5 hours to release the pattern designed on the Si wafer by removing the oxide layer. A 3D schematic of the fabrication process flow was shown in Figure 6.

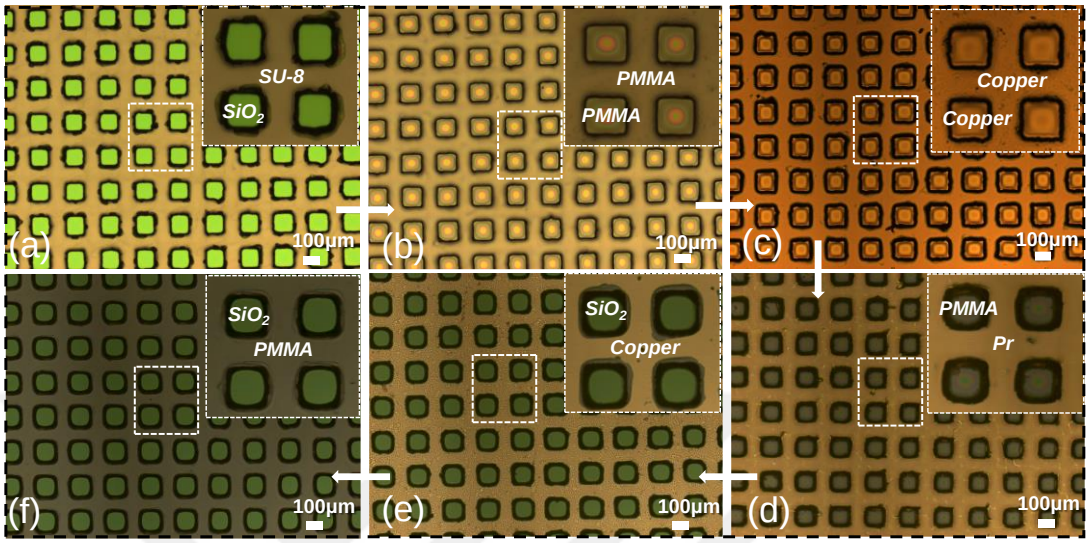

Figure 4 Microscope images of (a) Su-8 coated and patterned on SiO_2, (b) after PMMA coating on the patterned SU-8, (c) after copper deposition, (d) after photoresist coating and copper etching, (e) after applying oxygen plasma to etch PMMA from the exposed gaps, (f) after etching the top layer of copper.

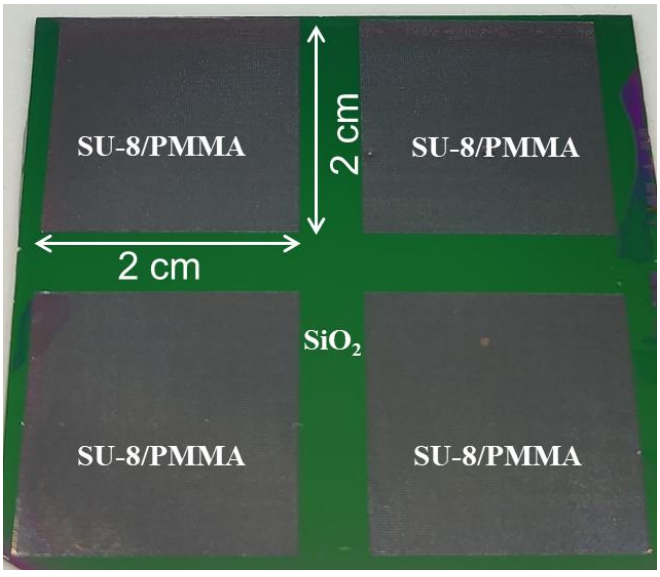

Figure 5 An optic image for an array of fabricated SU-8/PMMA before releasing from the silicon substrate.

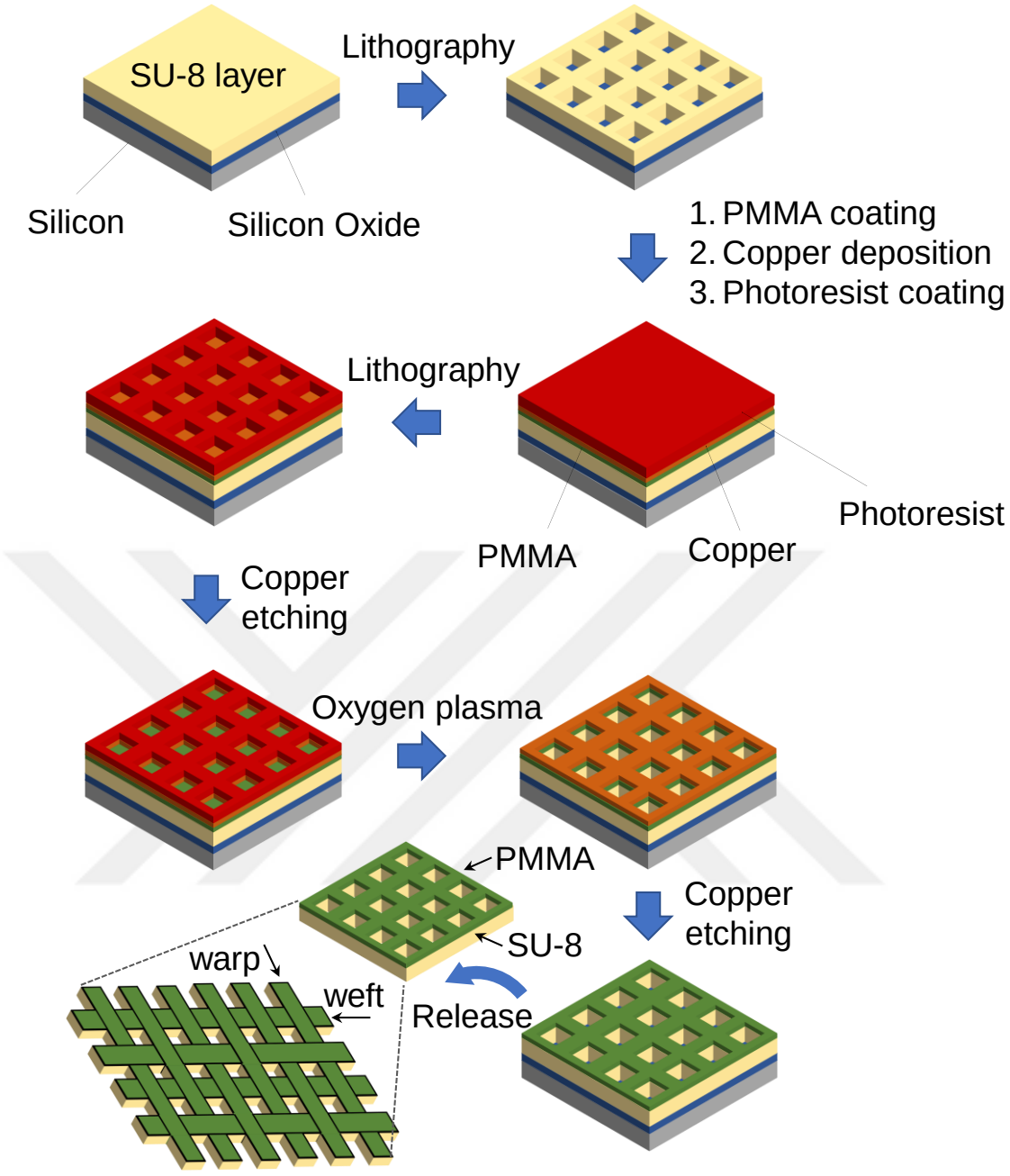

Figure 6 A 3D demonstration of fabrication steps of TPM electrode.

4.1.6 Electrode preparation and reduction

Graphene oxide (GO) was prepared using the modified Hummers method. The coating process includes drop-casting of diluted GO suspension on the SU-8/PMMA sample on a hydrophobic polytetrafluoroethylene (Teflon) surface. 0.3 ml GO was drop-casted, and

the sample was left at room temperature for a day to allow the evaporation of the solvent. Many attempts have been made to reduce the GO-coated TPM substrate such as chemical reduction and thermal reduction.

4.1.6.1 Chemical reduction of TPM electrode

For chemical reduction 0.027 g/ml of sodium borohydride ($NaBh_4$) was subjected to reduce the GO-coated TPM substrate, first the powder was dissolved inside DI water then the GO-coated TPM substrate was placed inside the solution, but directly the GO layer was delaminated from the substrate turning into small pieces and floating at the surface of the solution Figure 7a shows the sample after GO coating and Figure 7b demonstrates the GO coated sample during the $NaBh_4$ reduction attempt.

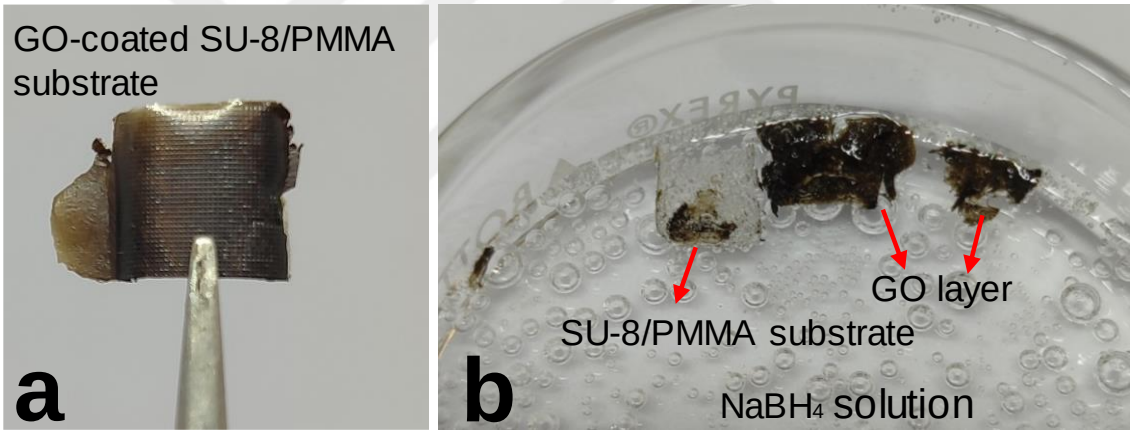

Figure 7 An optic image shows the sample (a) after GO coting, and (b) after sodium borohydride ($NaBh_4$) reduction.

4.1.6.2 Thermal reduction of TPM electrode

Thermal reduction was performed by putting the GO-coated TPM substrate inside a vacuum oven at 180 ºC for 3 hours resulted in a resistance of 0.5 kΩ but created a huge number of bubbles at the top surface of rGO layer with some defects leading the electrode to lose its conformality (Figure 8).

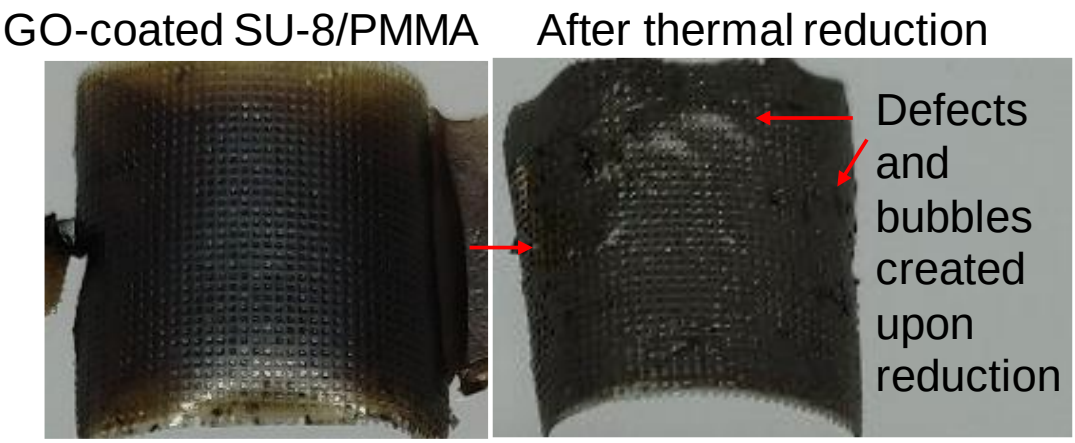

Figure 8 An optic image shows the sample before and after thermal reduction.

4.1.6.3 Green reduction of TPM electrode

To address the reduction issues an eco-friendlier vitamin C was employed. The reduction process includes preparing a solution of 0.35 g/ml L-ascorbic acid and DI water by mildly stirring them for 15 minutes at room temperature, followed by immersing the GO-coated sample into the prepared solution for three days at room temperature. Then it was cleaned using DI water to wash away excessive remnants of vitamin C and then left at room temperature for drying to form a TPM electrode (Figure 9a). This allowed successful reduction of GO without delamination and at the same time with high-quality surface. The final thickness of the electrode was between 85-95 μm. Furthermore, a 2×2 cm TPM electrode was weighed as 15.7 mg exhibiting a lightweight nature (figure 9b).

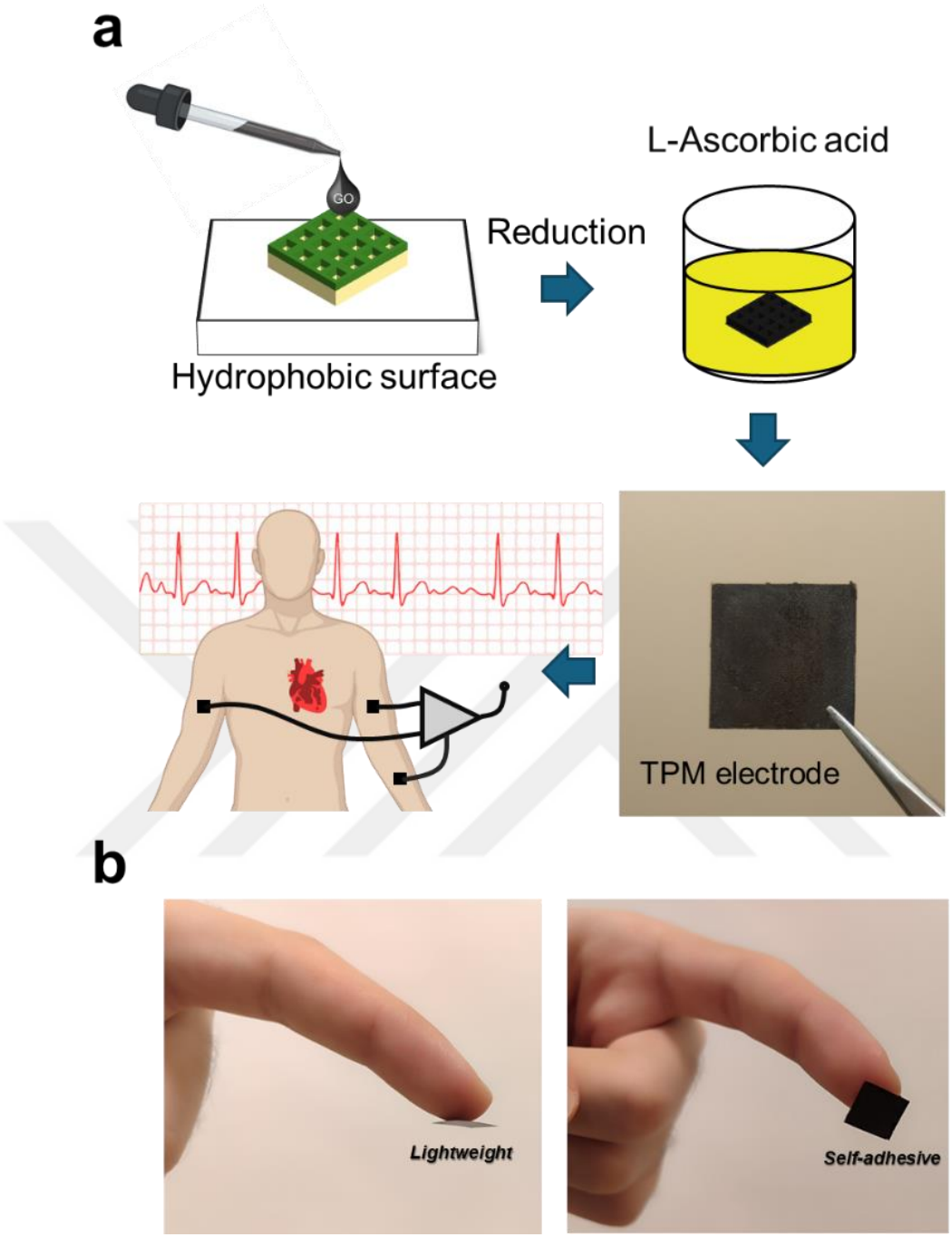

Figure 9 (a) A 3D schematic shows the green reduction process flow and the electrodes locations to record ECG signal, (b) Photos of the TPM electrode showcasing its lightweight nature and self-adhesiveness.

4.1.7 Wiring of TPM electrode

For quick prototyping, thin silver wires were connected to electrodes of 2 x 2 cm insize using silver paste. Owing to the electrode design, where there is a continuous conductive path between the two faces of the electrode, the wiring can be applied to one side of the electrode while the signal is taken from the other side. This wiring configuration in TPM electrodes prevents external electrical connection from touching the skin during measurement, thus ensuring better skin-electrode contact during electrode use, minimizing motion artifacts and inherently allowing high fidelity signal acquisition. Figure 10a shows an exploded view of the electrode topology consisting of different layers and Figure 10b demonstrates images of a fabricated electrode with and without wiring placed on the upper arm.

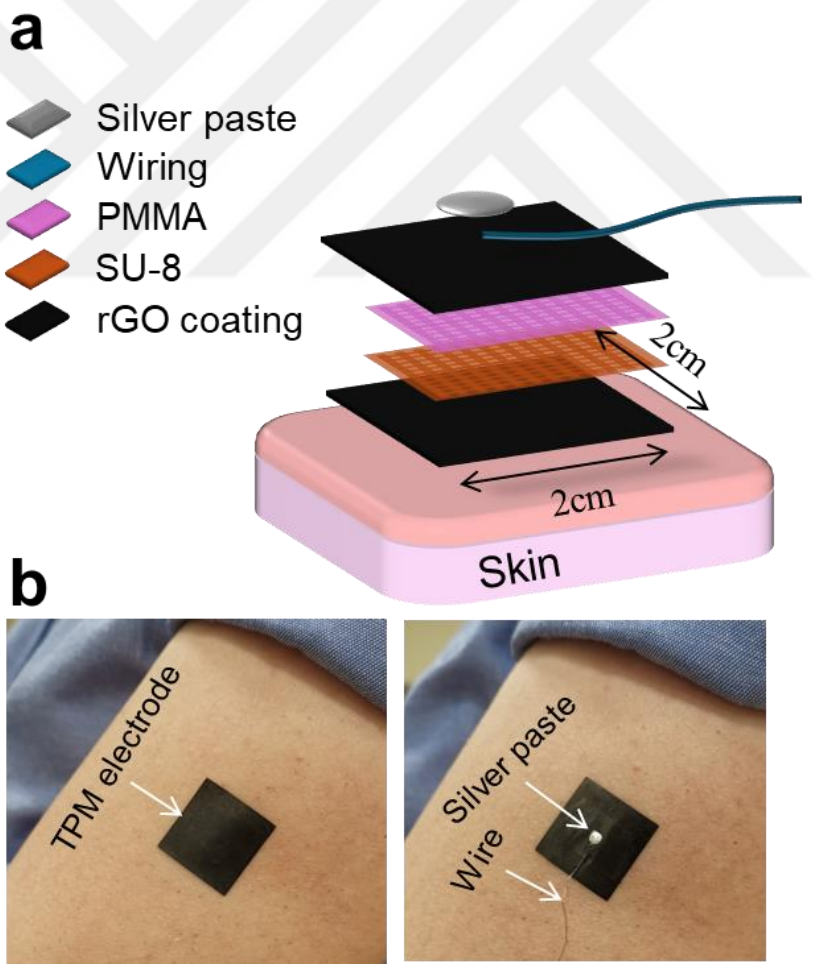

Figure 10 (a) Exploded view of a TPM electrode showing its inner layers, and (b) images of the electrode placed on the upper arm with and without wiring.

4.2 Characterization of TPM electrode

4.2.1 Evaluating the hard mask effect on PMMA purity

The impact of using a hard mask on the underlying PMMA layer was evaluated through Fourier-transform infrared spectroscopy (FTIR) (Nicolet iS10, Thermo Fisher Scientific). For this experiment three samples with the following multi-layer stack topologies were prepared: 1) Si/SiO2/PMMA, 2) Si/SiO2/PMMA/PR, and 3) Si/SiO2/PMMA/Cu/PR. First, the PR layer was removed from the second and third samples by UV flood exposure and development in AZ 726 MIF (Merck, Darmstadt, Germany) (Figure 11a). Next, the copper layer was etched from the third sample by a mixture of acetic acid, hydrogen peroxide, and DI water with a ratio of (1:1:18). Finally, the three samples were released using BOE for 12 hours to obtain structurally intact layers of PMMA.

In the first sample consisting of pure PMMA, the FTIR spectrum (Figure 11b) confirms the presence of the ester C=O bond around 1720 cm-1, and the band between 1120 cm-1 and 1220 cm-1 attributed to C-O stretching vibration. Likewise, two small peaks located in the 3000 cm-1 to 2900 cm-1 band of the PMMA spectra are assigned to –CH sp3, which are also in alignment with the previously published data [49,50]. We can observe the same peaks in the third sample's infrared spectra, which was prepared using the hard mask technique. This observation confirms that the hard mask (copper) does not leave any residues or affect the composition of PMMA afterwards. However, the spectrum of the second sample reveals both the characteristic peaks of pristine PMMA, along with a peak around 3350 cm-1 indicating O-H stretch due to Novolak resin; as well as, peaks between 1650 cm-1 and 1550 cm-1, confirming C=N stretching from naphthoquinone diazide, both of which hint at the chemical structure of photoresist [51,52] (Figure 12a). This result confirms that using photoresist as an etch mask to pattern PMMA is likely to leave hidden surface residues as evidenced by the identified peaks associated with the novolak resin and naphthoquinone diazide. The existence of photoresist residues on

PMMA surface is also visible by the reddish color of the sample prepared without the Cu hard mask (Figure 12b, 12c).

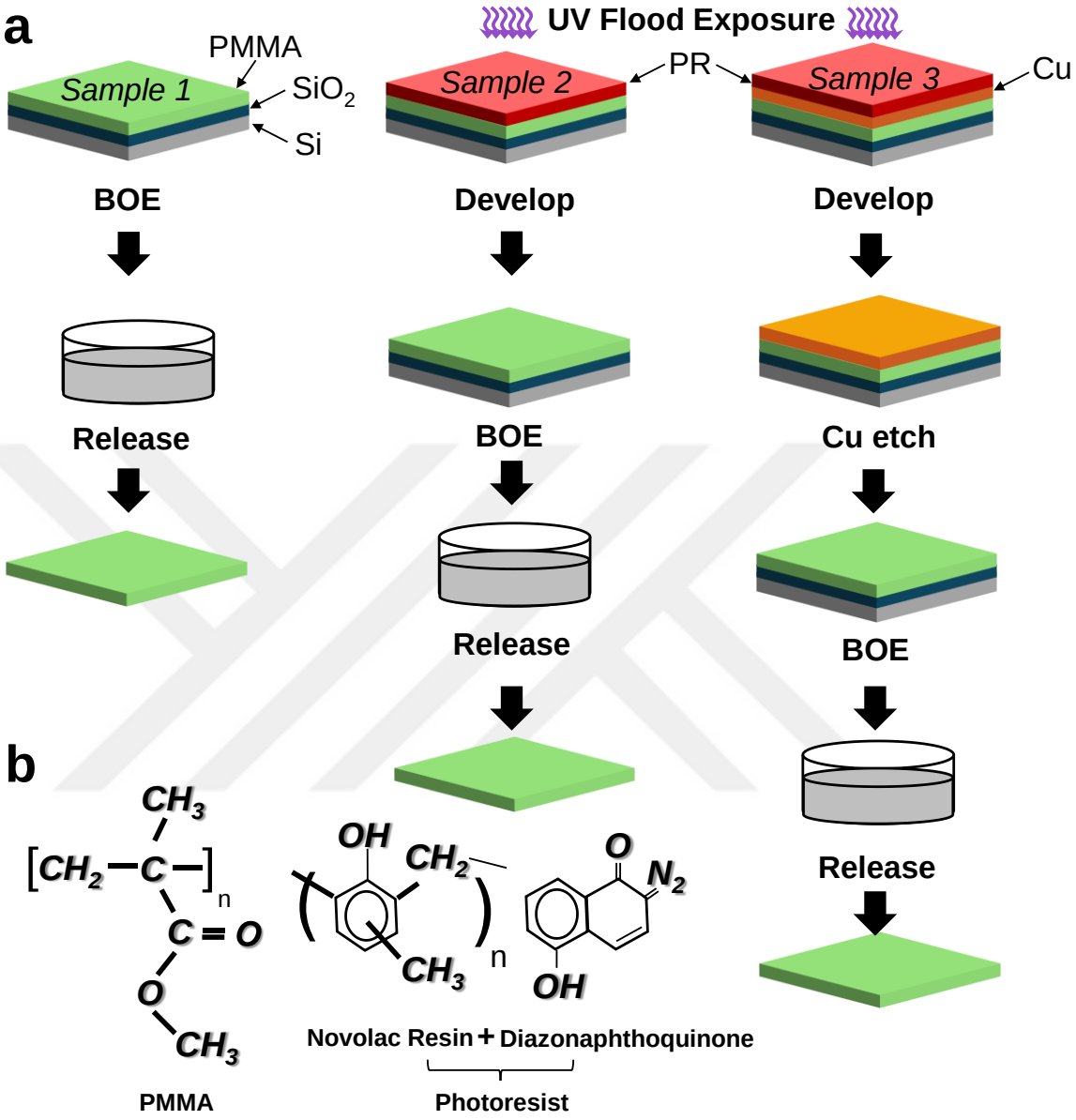

Figure 11 (a) 3D schematic of three sample fabrication steps to evaluate the purity of PMMA with and without utilizing the hard mask (Cu), and (b) PMMA and photoresist chemical structure.

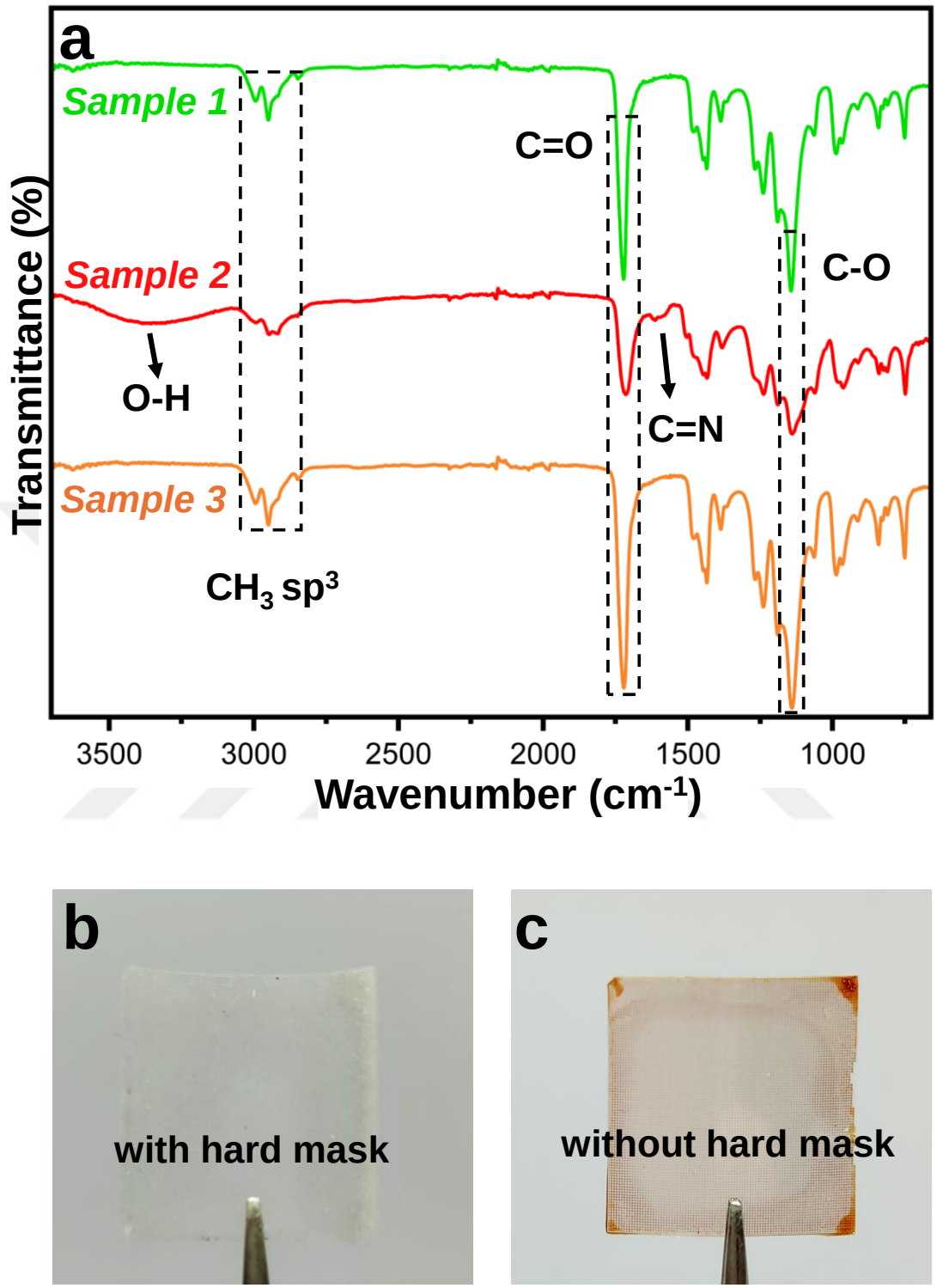

Figure 12 (a) Fourier-transform infrared spectroscopy (FTIR) analysis of three PMMA samples fabricated using different fabrication flows as Si/SiO_2/PMMA, Si/SiO_2/PMMA/Cu/Pr, Si/SiO_2/PMMA/Pr, respectively, and (b-c) Optic images comparing the SU-8/PMMA substrate with and without the implementation of the hard mask technique during fabrication.

4.2.2 The influence of the immersion duration on the electrode resistance

To choose the optimum time for immersion of the electrode into vitamin C, one TPM substrate 2×2 cm was coated with GO and left to dry then cut into 4 pieces 1×1 each. After that, the four pieces were placed inside the vitamin C solution and every 3 days for a total of 12 days, one piece was taken out of the solution and left one day to dry at room temperature then the resistance was measured. The resistance was measured as 4.7, 2.7, 0,83, and 0,67 kΩ in the electrodes left inside the reduction solution for 3, 6, 9, and 12 days, respectively (Figure 13a). The results demonstrate that the resistance drops were 42.55%, 82.34%, and 85.74% after 6, 9, and 12 days, respectively, in contrast to 3 days. The significant drop in resistance occurred after 9 days in the reduction solution, and it stabilized after 12 days. Therefore, to achieve a resistance below 1 kΩ for the GO film, 9 days was selected as the optimal duration in the vitamin C solution.

Further, after selecting the optimal duration, the resistance of the electrode was measured every 10 days for one month, the result demonstrated a decreasing trend from 0.83 kΩ to 0.43 kΩ in one month (Figure 13b). With a rapid fall during the first 10 days and remaining relatively stable thereafter. This decreasing trend in resistance is likely attributed to the gradual removal of oxygen functional groups from the rGO layer as time passes at room temperature.

These results indicate that a 3-day treatment in the reduction solution was sufficient to convert the GO to rGO with a resistance of around 5 kΩ. However, increasing the number of days in the reduction solution can further reduce the resistance, resulting in a more sensitive rGO film, without negatively affecting the electrode quality.

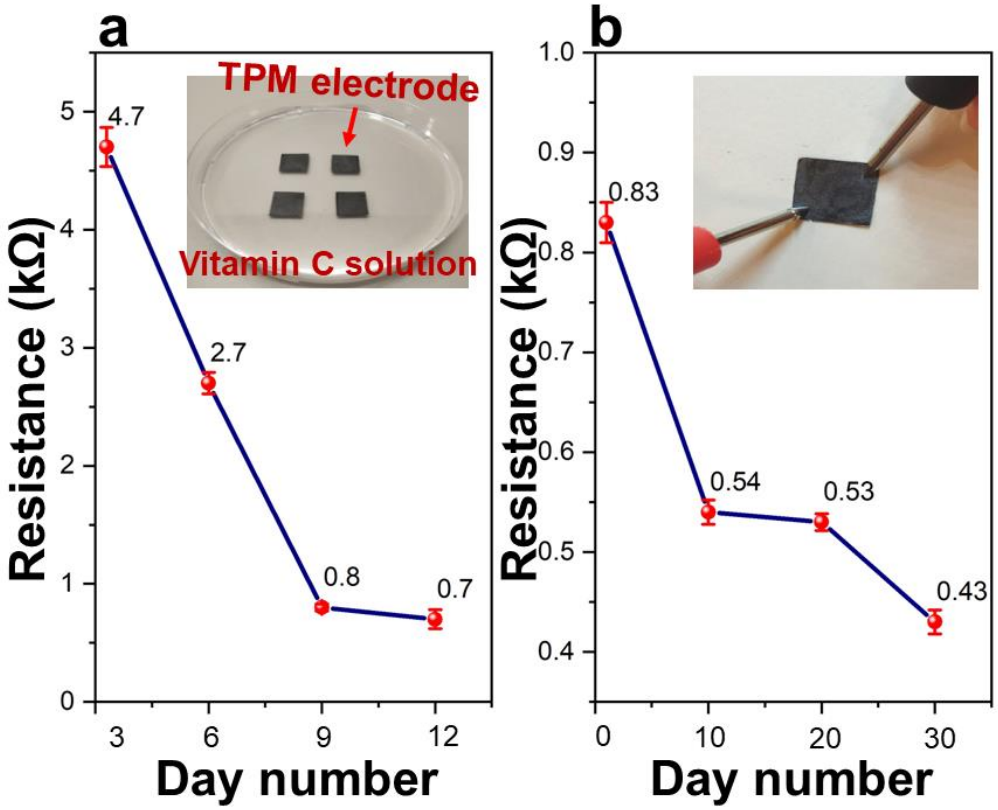

Figure 13 (a) Resistance measurement of TPM electrode immersed in vitamin C solution for 3, 6, 9, 12 days, respectively, (b) measuring resistance of 9-days-immersed TPM electrode in the vitamin C solution, for a duration of one month.

4.2.3 Scanning electron microscopy (SEM) of TPM electrode.

rGO-coated TPM substrate was performed to inspect the conformality of the rGO coating on the "artificially-weaved" microstructured PMMA surface by SEM (Zeiss Gemini Supra 35 VP, LEO, Germany) (Figure 14). The images verify that the gaps between stripes are well-filled with rGO homogenously, effectively providing an electrical connection between the top and bottom faces of the electrode. This is advantageous to realize a reliable skin-electrode contact and highly feasible for electrical wiring purposes, facilitating the acquisition of biopotential signals without disturbing the skin-electrode contact.

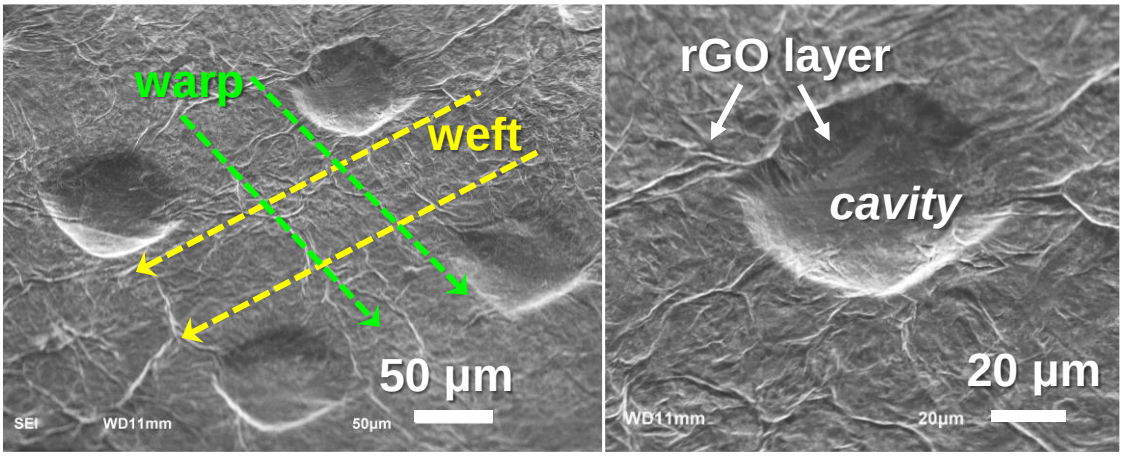

Figure 14 Scanning electron microscopy images (SEM) of the TPM electrodes.

4.2.4 The impact of the square pattern on rGO attachment.

To assess the impact of the "weft-warp"-like microstructured surface, a sample was fabricated following the previous procedure but without the patterning of SU-8 and PMMA layers. Subsequently, GO was applied to the sample using the drop-casting method and then reduced rGO via the vitamin C reduction process. The influence of employing a smooth substrate without gaps on the adherence of the rGO layer was illustrated in Figure 15. While the GO layer adhered fully to the unpatterned SU-8/PMMA substrate due to the drop-casting method, the rGO layer detaches upon reduction and the sample rinse. The "weft-warp"-like microstructured surface enables the uniform attachment and layering of the rGO layer to the PMMA/SU-8 substrate. These findings indicate that the "weft-warp" pattern stabilizes the uniform attachment of the rGO layer onto polymer-based composite substrates.

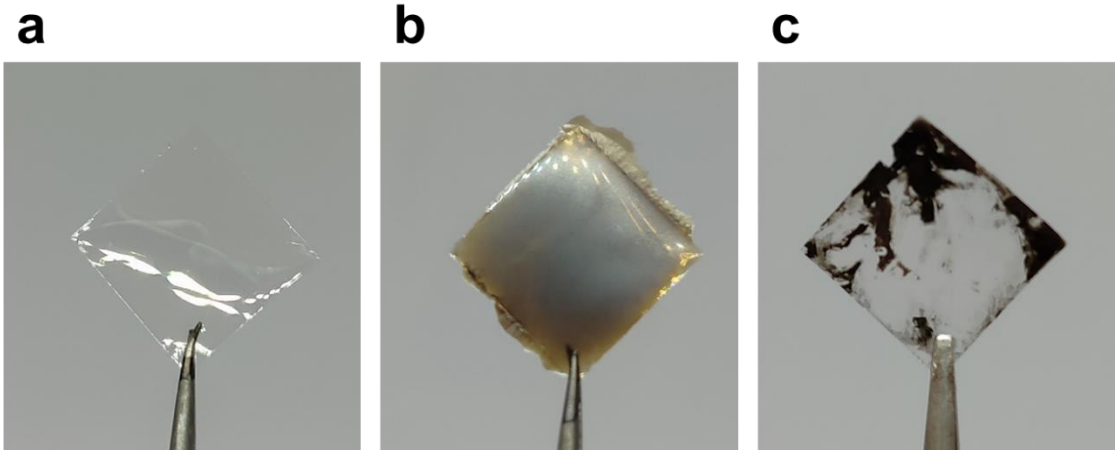

Figure 15 The SU-8/PMMA electrode fabricated without the squares pattern (a) before coating with GO, (b) after GO drop-casting and drying on a hydrophobic surface, (c) after 3 days of vitamin C reduction.

4.2.5 Raman spectroscopy

Raman spectroscopy (Renishaw, Wotton-under-Edge, UK) was performed with a 532 nm excitation laser and 1 cm^{-1} spectral resolution to confirm the transition of GO to rGO by the reduction agent, ascorbic acid. Raman shifts of graphene-based materials show two peaks referred to as the D and G bands, varying from 1308 to 1375 cm^{-1} for GO and 1536 to 1599 cm^{-1} for rGO. The G-band is commonly associated with the presence of C-C bond in sp^2 of carbon atoms in the 2D hexagonal plane. As a result, the D and G band intensity ratio (ID/IG) illustrates the reduction extent that results from the restoration of graphene structure and the removal of oxygen atoms from GO. As shown in Figure 16a, while the ID/IG is 0.89 for GO, it has increased to 1.23 after the reduction process with ascorbic acid. This confirms the reduction of GO to rGO and restoration of graphene structure due to the removal of oxygen atoms from GO. Figure 16b shows that the GO-coated surface preserves uniformity after the reduction process.

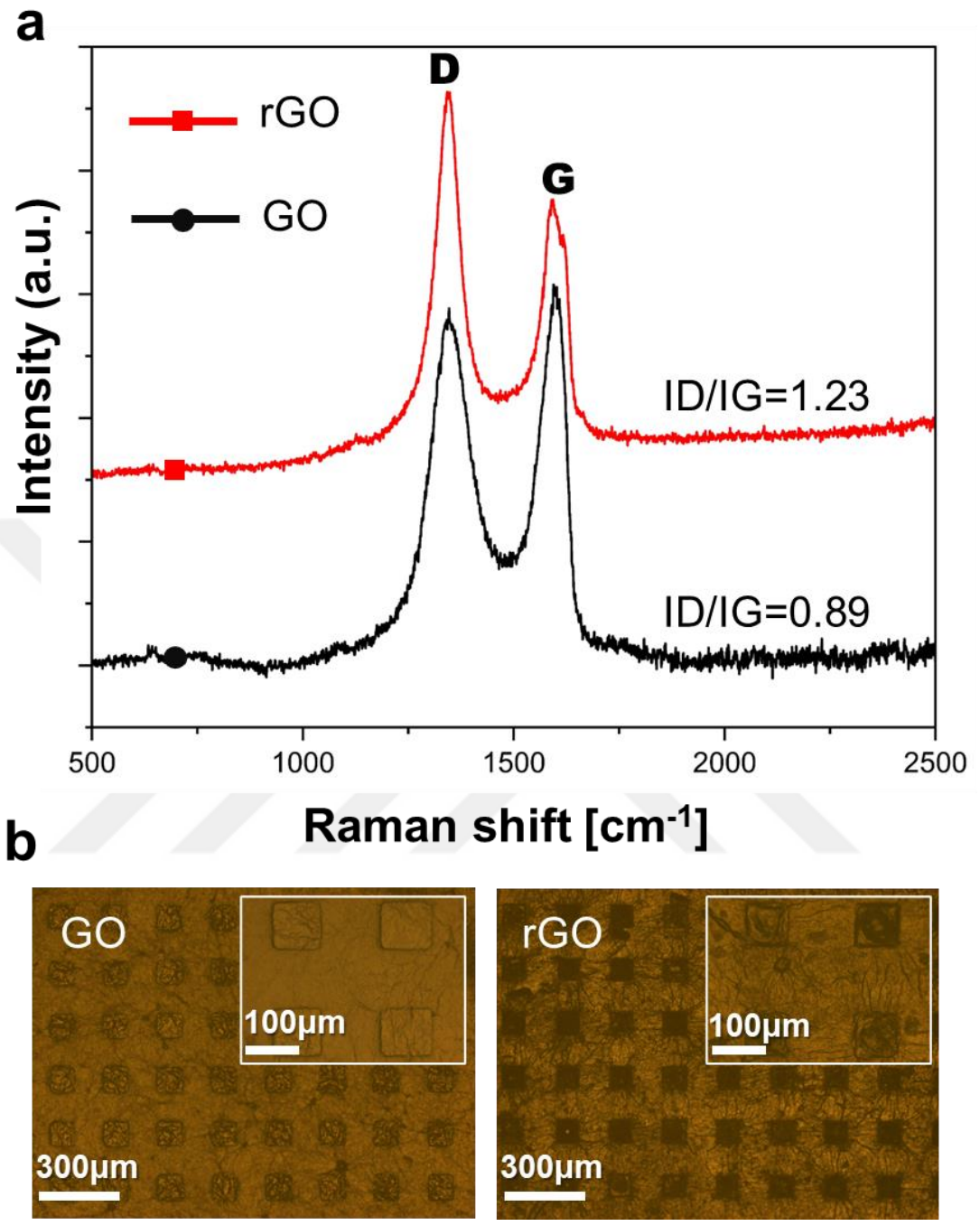

Figure 16 (a) Raman spectra of graphene oxide (GO) and reduced graphene oxide (rGO) traces, (b) Optical microscope images of TPM electrode before and after GO reduction.

4.2.6 Skin-electrode impedance

A measurement circuit based on a previously developed design [31], [53] was built to find the impedance of TPM electrodes and to compare it with commercial Ag/AgCl electrodes. Three electrodes were placed on a 25-year-old participant's forearm, who has

a body mass index (BMI) of 24.9. The setup is shown in Figure 17. A sinusoidal current was applied by the Howland current pump through the skin with an increasing frequency of 1Hz-1kHz in 5 seconds intervals. By dividing the voltage drop between the target and counter electrodes by the current from the reference electrode, the skin-electrode impedance was calculated. The governing equation of skin-electrode impedance is also formulated in Figure 17. Z_C is the contact impedance between the skin and electrodes, I is the generated current, V_{d1} is the voltage drop on Z_c, V_{d2} is the voltage drop on the resistance R (Equation 4.1). As shown in Figure 17 the impedance of the Ag/AgCl varies between 20.83 kΩ and 5.42 kΩ, respectively. On the other hand, TPM electrodes vary in the range of 35.56 kΩ and 7.83 kΩ. Although there is a slight difference in impedance values, such differences are not critical and the skin-electrode impedance of the electrodes is still well within the range of contact impedance, this is necessary for high-performance biopotential records.

$$Z_c = \frac{V_{d1}}{I} = \frac{V_{d1}R}{V_{d2}} \tag{4.1}$$

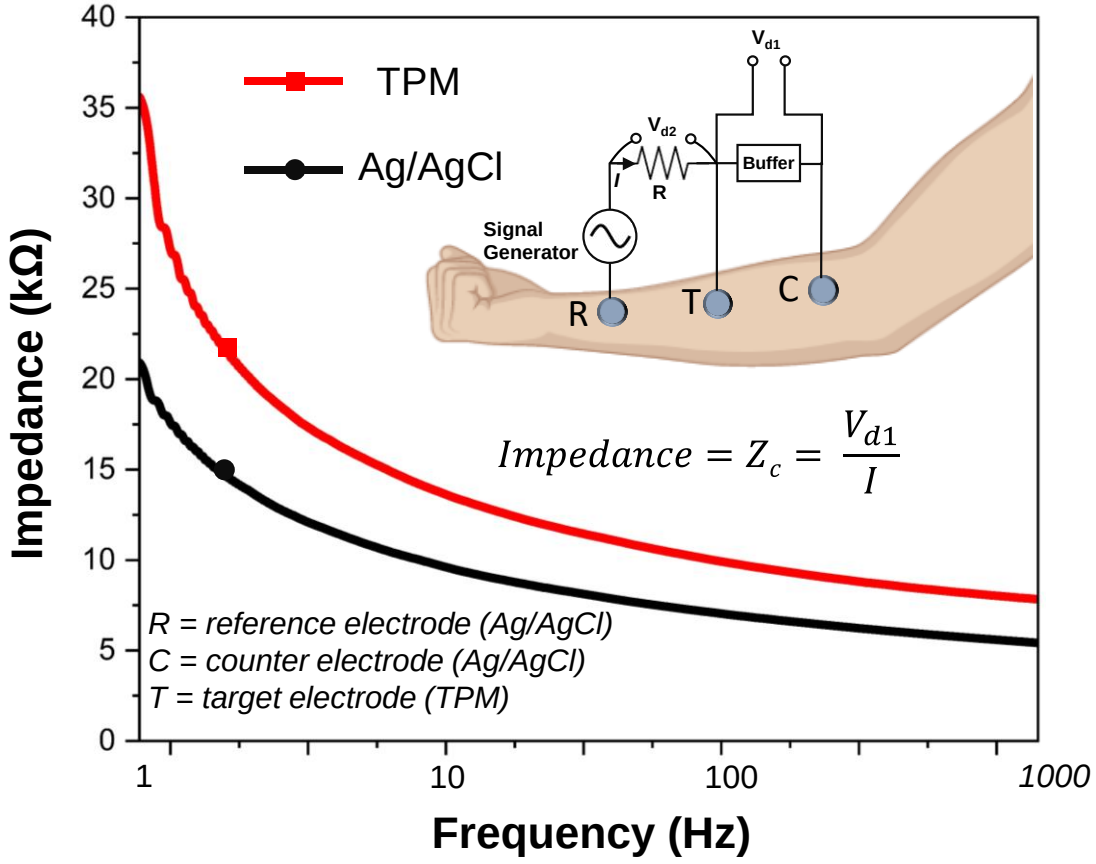

Figure 17 Skin-electrode contact impedance in relation to frequency variation with the inset of the experimental setup for the TPM and Ag/AgCl electrodes.

CHAPTER 5.

RESULTS AND DISCUSSION

5.1 ECG signal recording

Two electrodes were placed on each arm along with a reference electrode to record ECG in lead-1 configuration. To benchmark the performance of the fabricated TPM electrodes, a commercial biopotential data collection unit (Cyton Board, OpenBCI) was used. The recorded data was processed and filtered using custom-written MATLAB scripts. A notch filter was first applied to eliminate the powerline interference at 50 and 100 Hz. Then a bandpass filter was applied to remove noise outside the frequency range of 5 Hz to 50 Hz. Lastly, a fifth order moving average filter was applied to smooth the signal. The built-in correlation function in MATLAB was applied for 10 s of data to assess the similarity between simultaneously recorded ECG signals from Ag/AgCl and TPM electrodes. To assess the signal quality, signal-to-noise ratio (SNR) and RMS noise scores were calculated. Energy around the QRS complex was attributed as the "signal", while the remaining baseline fluctuations including the isopotential line were considered as "noise" (Equation 5.1).

$$SNR[dB] = 20 \log \left(\frac{|E_{RRS}|}{E_{noise}}\right) \qquad (5.1)$$

5.1.1 Evaluation of the performance of TPM electrode to record ECG signal

This experiment was performed on a 32-year-old participant with no known cardiovascular disease history. The participant was instructed to sit still under static conditions on a chair in front of the data collection setup. TPM electrodes were in lead-

I configuration and they were fixated on the arm using the self-adhesive ability of the electrodes without using any extra materials, The self-adhesive ability of the electrodes is attributed to the ultrathin structure of the electrode due to Van der Waals and Capillary interactions [37,54] and likely due to the concave structure of the cavities [55], Figure 18a demonstrates the 2×2 cm TPM electrode placed on the participant's arm undergoing different movements to assess its self-adhesiveness. Even under conditions of severe movement, the electrode shows extraordinary adhesiveness to the skin. Additionally, Figure 18b showcases the real-time acquisition of the ECG signal during severe hand movement for both the Ag/AgCl and TPM electrodes. As the electrode position highly affects the signal morphology, wet Ag/AgCl electrodes were placed right next to the TPMs to make a fair comparison between the two. The PQRST complex was clearly visible in the collected datasets. Figure 19 shows almost two identical ECG traces recorded with the TPM and Ag/AgCl electrodes that exhibit a correlation of %98.84.

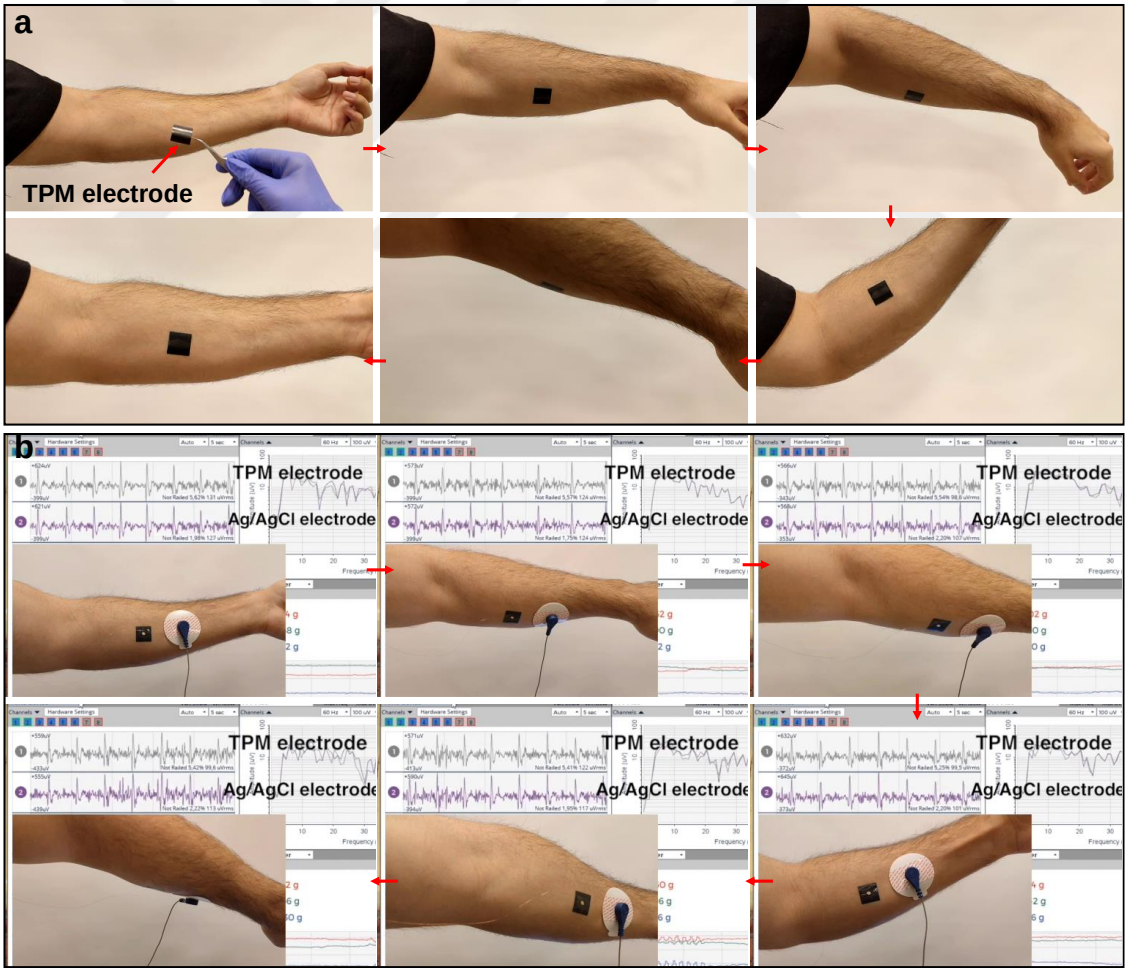

Figure 18 (a) Optical images shows the self-adhesiveness of a TPM electrode by applying severe movement to an electrode placed on the arm, b) Recording the ECG signal during arm movement for Ag/AgCl and TPM electrodes.

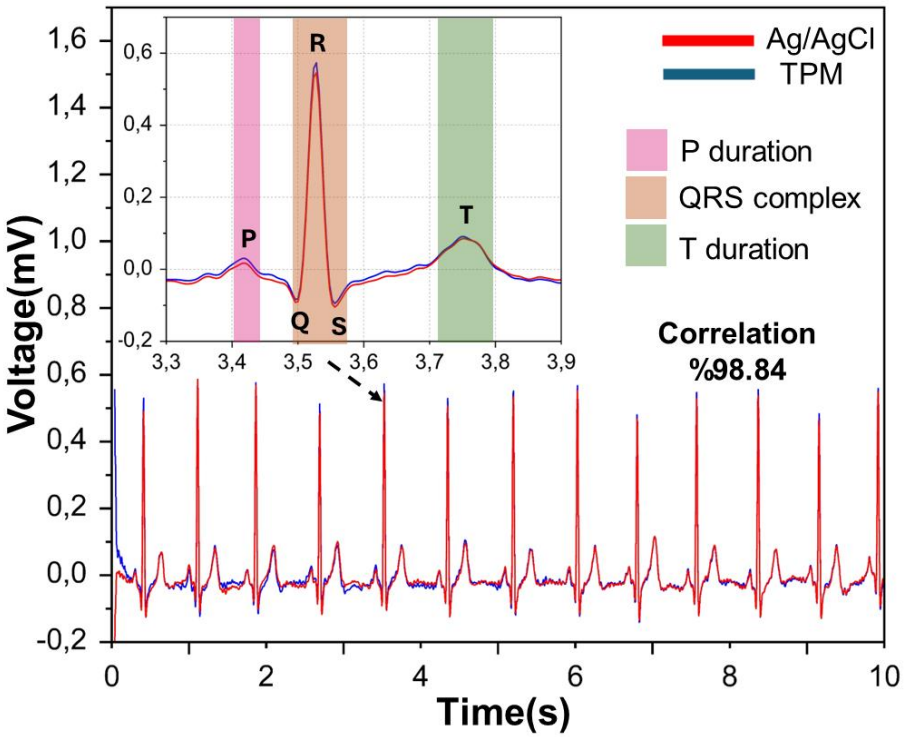

Figure 19 Simultaneous ECG recording with TPM and Ag/AgCl electrodes.

5.1.2 Evaluation of the self-adhesive ability of TPM electrodes in long-term ECG recording

To assess the electrode's self-adhesive ability in long-term ECG recording (i.e., 30 minutes), no adhesive materials were used during this experiment to observe the self-adhesiveness of TPM electrodes. The participant was again instructed to sit down in front of a monitor, and the data was collected while he was watching a half-hour-long TV series episode in his preference, where he occasionally twitched his arms voluntarily to relieve his arm muscles. Ag/AgCl electrodes were placed next to TPM electrodes on both upper arms to perform synchronous data acquisition. In Figure 20 five-second temporal windows, extracted from the 30-minute-long electrocardiogram recording, at every 6-minute intervals and its multiples are shown.

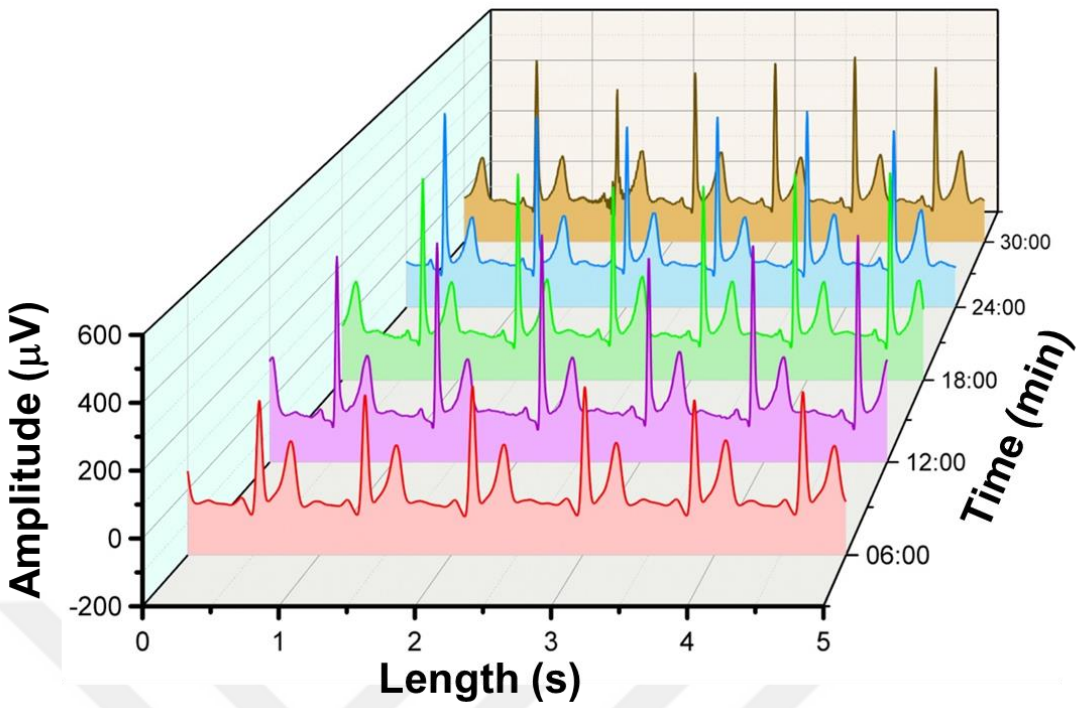

Figure 20 ECG acquiring for 30 minutes simultaneously for TPM electrodes.

SNR scores and RMS noise of TPM and Ag/AgCl electrodes were calculated for the 30-minute-long ECG signal. The results showed are higher signal in all the five signal segments of upto 0.7 dB. The mean RMS noise changed from 41.92 to 46.6 μV, and SNR changed from 21.06 to 26.17 dB for the TPM electrodes; while Ag/AgCl displayed mean RMS noise from 43.41 to 47.8 μV and SNR changed from 20.81 to 25.88 dB (Figure 21). The relative standard deviation (RSD) is calculated as %4, which demonstrates the outstanding stability of the TPM electrodes even in long ECG recordings.

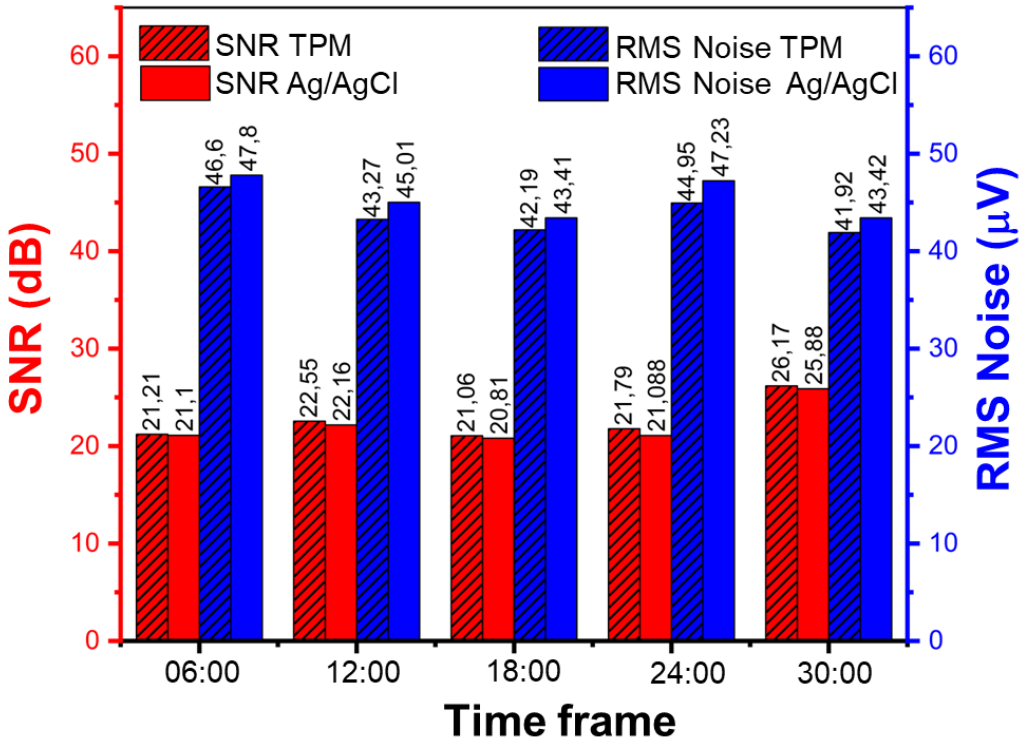

Figure 21 signal-to-noise ratio and RMS noise for the five signal segments of 30-min long ECG signal.

5.1.3 Evaluation of the waterproof ability of TPM electrodes

To investigate the waterproof surface of the TPM electrodes they were kept immersed in water for five days. Each day, they were used to collect data from the same participant, and signal degradation was observed. Figure 22a shows these ECG recordings acquired with the TPM electrode for 6 consecutive days, where the electrode was kept immersed in water for 5 days. The SNR score before wet immersion was calculated as 15.94 dB. Then from the first day to the last the SNR dropped from 17.92 dB to 16.029 dB with relative standard deviation of 15%, where we attribute to experimental measurements errors. The RMS noise before immersion was calculated as 43.82 μV, and then from first day to the last it ranged from 44.79 to 47.087 μV with a relative standard deviation of %9.1 (Figure 22b). The stability of the SNR and mean RMS noise scores verifies the functionality of TPM electrodes in wet environments and proves their durability.

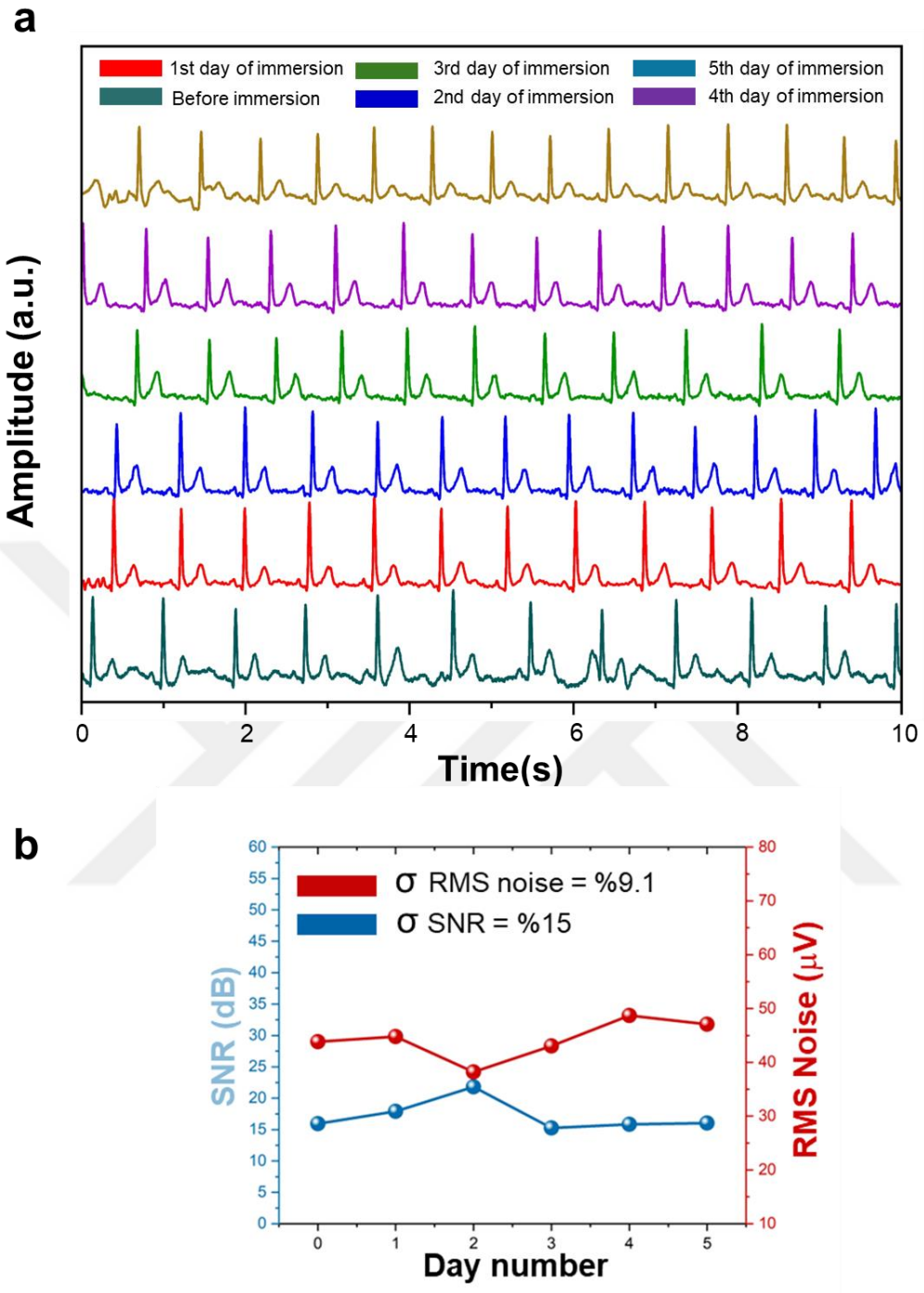

Figure 22 (a) The waterproof capability of TPM electrodes are demonstrated by consecutive ECG recordings of 10 s each during 5 days of immersion into water; (b) signal-to-noise ratio and RMS noise of the ECG signal taken before and during a 5-day period with the TPM water-immersed electrodes.

5.1.4 Evaluation of the TPM electrodes' water resistance

This experiment was conducted to assess the electrodes' water resistance capability in wet environments (e.g., perspiration during intense exercise). First the sessile drop method is used to determine the contact angle and verify the waterproof ability of the electrodes, where contact angles above 90º indicate that a sample is hydrophobic and therefore waterproof [56]. In this thesis (Theta Lite optical tensiometer) with a video-camera system and computer software was used to measure the contact angle. Accordingly, a drop of water was applied onto the TPM electrode surface and then the contact angle was measured in the first 10 s after a droplet was formed on the surface. TPM electrodes on average showed a contact angle of ~71º between the drop and the electrode surface (Figure 23a). The partially hydrophobic surface of the TPM electrode with of ~71º contact angle allows it to display some waterproof capability. Photos of the electrode before and after five days of constant water immersion show minimum visual deformation on the rGO surface (figure 23b). SEM images of the surface after five days of water immersion indicate only small deformations occurring on the surface as empty spots (figure 23c). Further, The 5-day ECG acquisition using TPM electrodes immersed in water reveals that the presence of empty spots on the electrode doesn't result in any signal disturbances, which assures the reusability of the TPM electrode under intense wet conditions.

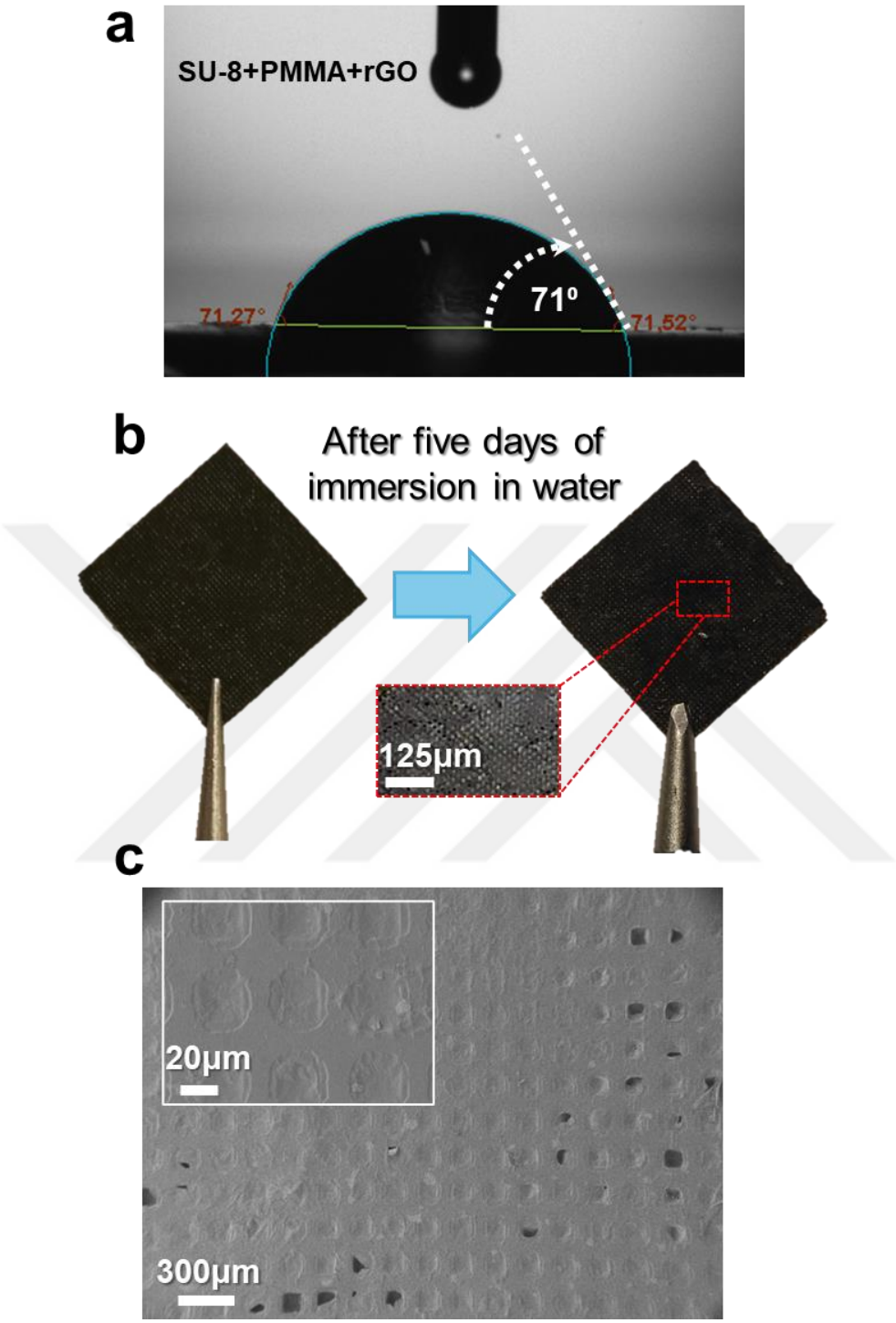

Figure 23 (a) Contact angle of the TPM electrode, (b) Images of the TPM electrode in dry state and after immersing the electrodes into the electrodes inside water for 5 days, (c) SEM image of the TPM electrode after remaining in water for 5 days.

5.2 Mechanical properties of TPM electrode

Several experiments were performed to evaluate the mechanical and electrical stability of the electrode even in harsh continuous use conditions.

5.2.1 Manual flexibility test

A manual flexibility test was carried out for TPM electrodes where they undergo a gradual force applied by compressing an electrode initially aligned parallel to the vertical direction with two fingers. Accordingly, starting from the initial condition when the TPM electrode surface makes zero degrees with respect to the vertical direction, the electrode is bent by compressing in between two fingers such that the bending angle (θ) varies from varies from 25° to 75° (Figure 24), up to 75° the TPM electrode is compliant and can recover the deformation. This phenomenon verifies the flexibility of the electrode and its ability to adapt to uneven skin surfaces. However, when the electrode is bent further to 75◦, the TPM structure breaks apart by cradling at high-stress locations.

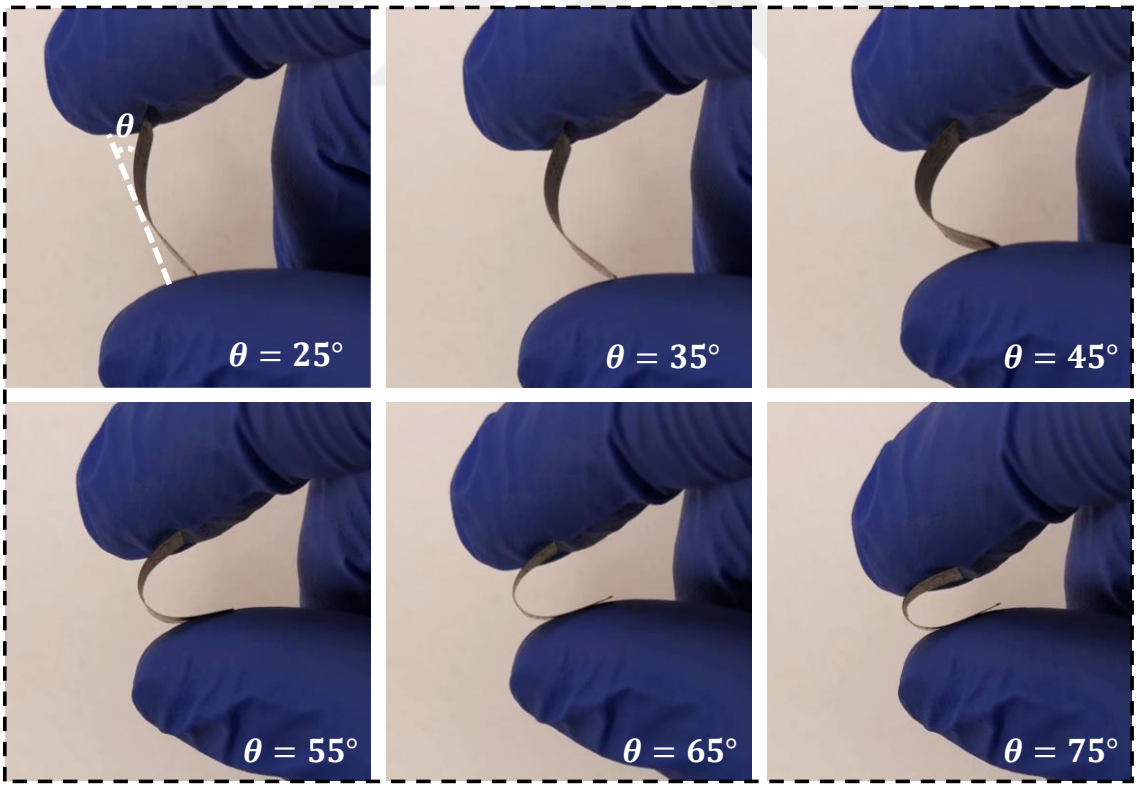

Figure 24 Flexibility test applied by manually bending the electrode angles from 25° to 75° degrees.

5.2.2 Assessment of the mechanical deformation on TPM electrodes performance

The performance of the electrodes was verified in cyclic operation where they were subjected to successive bending cycles to observe the effects of mechanical deformations on the physical surface. The experiment was performed by placing the TPM electrode on polyethylene terephthalate (PET) film and fixing it on a voice coil actuator which can be driven with different waveforms to adjust the bending angle during repetitive compression as shown in Figure 25a. SEM images were obtained in each phase to assess the degradation level on the rGO surface after each experimental cycle, in Figure 25b, the SEM images of the electrode before bending are shown. Figure 25c demonstrates the electrode after 100 bending cycles, and Figure 25d shows the electrode after 200 bending cycles. The SEM images indicate that there is not much change after 200 bending cycles. The stability of the electrode was further demonstrated by acquiring ECG after 200 bending cycles. In this experiment, the TPM electrodes before and after 200 bending cycle were placed beside each other and the ECG signal was recorded (Figure 25e). The correlation between the two signals showed a high correlation up to 99.48%. The SNR was calculated as 24.1 dB and 23.85 dB from TPM before and after the 200 bending cycles, respectively. Therefore, the 200 bending cycles have a minimum effect on the electrode's performance in acquiring ECG signals.

Likewise, the change of electrode sheet resistance (Rs) with respect to bending was quantified with a four-point probe unit (C4S, Cascade Microtech, Beaverton, Oregon, US) before and after bending up to 200 cycles. The baseline Rs prior to bending was measured as ~103 Ω/□ which increased to ~179 Ω/□, after 4 bending cycles with 200 repetitions of compression up to 45°, Table 1 summarizes the change of R_s with bending cycle. The slight increasing trend in sheet resistance and the SEM images revealed no visible damage on the rGO surface after 100 bending and a very subtle change in rGO surface after 200 bending cycles.

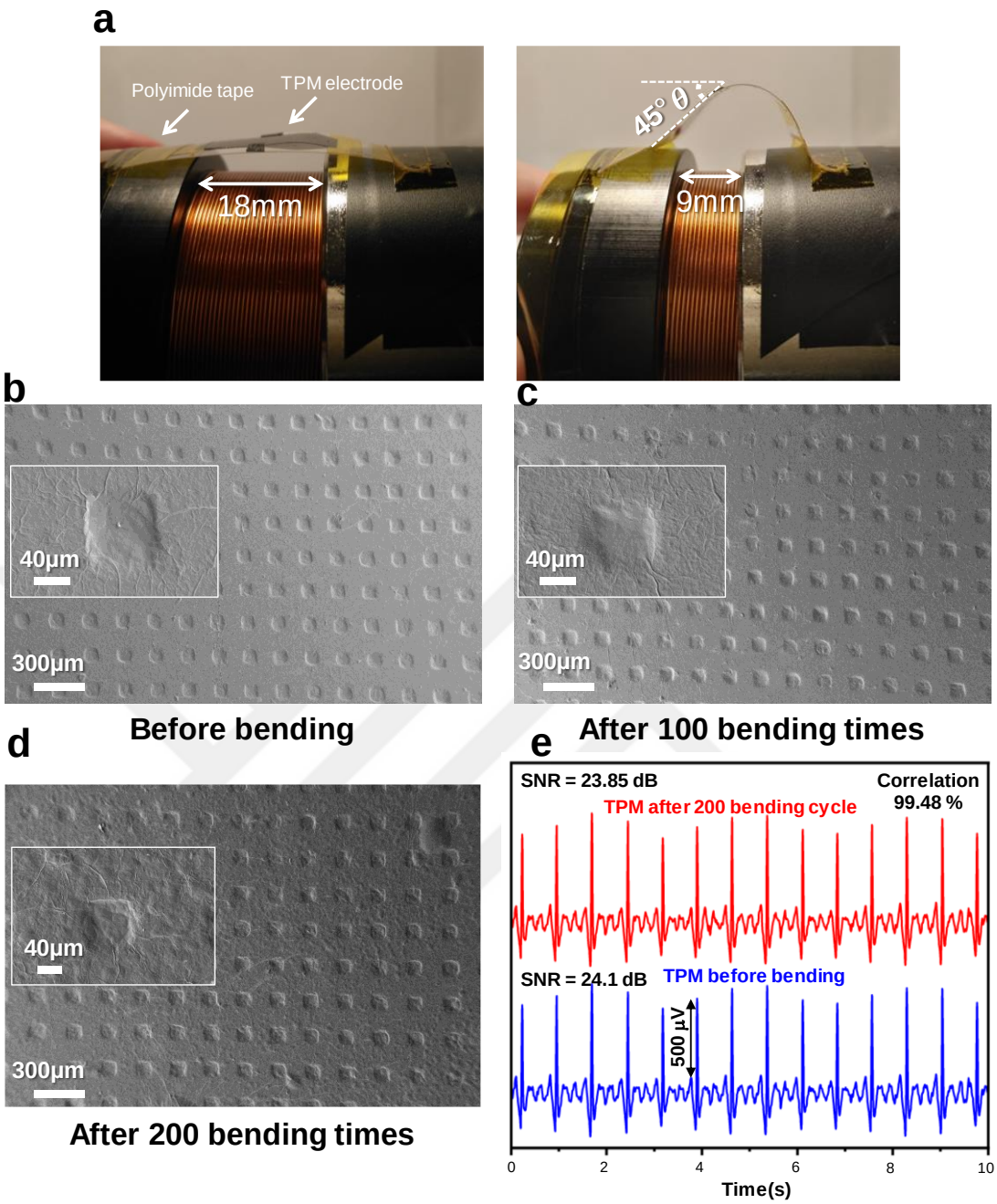

Figure 25 (a) Bending test setup, (b,c,d) SEM images of the electrode before the bending, after 100, and after 200 times bending applied, respectively, (e) 10 s windows show ECG signal was taken simultaneously of TPM electrodes before and after the 200 bending cycle.

Table 1. Change of sheet resistance (R_s) with bending

No. of cycles	Sheet resistance (R_s) (Ω/□)	$\Delta R/R$ (%)
0	103.51±3.87	0
50	118.91±11.128	14.88
100	132.61±8.35	11.52
150	158.55±12.4	19.56
200	178.94±31.68	12.86

5.2.3 Tensile test

To evaluate the effect of the PMMA layer on the mechanical properties of the SU-8 substrate, a tensile test was performed (Mark-10 M7-200) with a 50 N load cell and resolution of 0.2 N was used. The samples were fabricated in a rectangular shape with a size of 450 × 50 mm with the previously described process without patterns on the sample for precise measurement, then each sample was placed on the fixture of the device with a gap measured manually for the strain test. A crosshead speed of 0.8 mm per minute was applied to the samples, and the test was not stopped until the sample was broken, Figure 26 demonstrates tensile test was performed on one SU-8/PMMA sample until it breaks. Load and travel distance were measured, from which strain and stress data were calculated from equations 5.2 and 5.3, respectively where ε, L, F, A are the strain, length, force, and area of the sample, respectively.

$$\varepsilon = \frac{\Delta L}{L} \qquad (5.2)$$

$$stress = \frac{F}{A} \qquad (5.3)$$

The tensile stress and strain data were obtained based on the original cross-sectional area and length of the samples. The test was repeated for samples of SU-8 and samples of SU-8/PMMA for at least 3 each. Young's modulus was determined by the slope of the stress-strain graph. The results revealed a slight change in Young's modulus from 1.8±0.81 GPa to 1.9±0.32 GPa after the inclusion of the PMMA layer. The measured Young's modulus is slightly different from the SU-8 manufacture datasheet value of (2 GPa), which is attributed to fabrication conditions such as UV exposure time and temperature, [57, 58]. To assess the mechanical prosperities of the SU-8 substrate before and after adding the PMMA layer, toughness is calculated by the area under the stress-strain graph. The results offered an increase from 0.47±0.036 MJ/m^3 to 0.98±0.15 MJ/ m^3 which is a significant increase of 108.5% in the SU-8/PMMA substrate toughness. The toughness represents the amount of energy the sample can bear before fracture [59]. Thus, the new composite can withstand more load before it fails, indicating enhancement of the mechanical properties after adding the PMMA layer. Likewise, the strain and ultimate strength of the SU-8/PMMA composite showed an increase of 66.7% and 37.7%, respectively. Table 2

summarizes the SU-8 and SU-8/PMMA mechanical properties.

Based on the measurement results, the most robust electrode is SU-8/PMMA composite TPM, where the thin layer of PMMA makes the electrode more robust, leading to a lower risk of breaking. Even though the PMMA layer thickness is 300 nm, the effect of the acrylic-based flexible PMMA is dominant here. Adding the PMMA layer makes the electrode use repeatable and shows a promising result for wearable ECG monitoring.

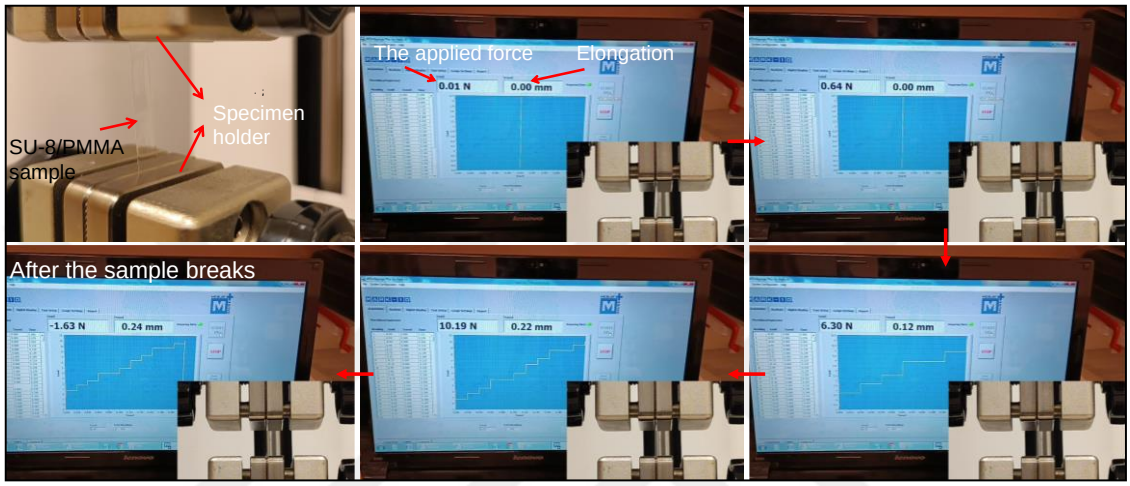

Figure 26 Tensile test experiment for SU-8/PMMA sample.

Table 2. Summary of mechanical properties of the Su-8 and Su-8/PMMA

Mechanical properties	**SU-8**	**SU-8/PMMA**	**% Change**
Young's modulus (GPa)	1.8±0.81	1.9±0,32	5.5
Strain	0.024±0.0022	0.04±0.0066	66.7
Ultimate Strength (MPa)	40.41±1.14	55.63±6.74	37.7
Toughness (MJ/m^3)	0.47±0.036	0.98±0.15	108.5

CHAPTER 6.

CONCLUSION AND FUTURE WORK

Inspired by the graphene-textile electrodes in this thesis, flexible artificial, textile-like polymer-based microstructured (TPM) electrodes were developed. We demonstrate the self-adhesiveness and flexible nature of TPMs similar to duct tapes that render them suitable for wearable, long-term biopotential monitoring, specifically for electrocardiography (ECG). Poly (methyl methacrylate) (PMMA), a widely used polymer in the textile industry, and SU-8, a negative photoresist polymer, were used as the core materials and underwent microfabrication steps to achieve a textile-like structure of 100 um gaps and 100 um spacings. To establish the conductivity of the fabricated electrodes a simple reduction process was introduced to the graphene oxide (GO) compromising the usage of Vitamin C (L-Ascorbic Acid), an organic and nature-friendly reduction agent. Different characterizations were performed on the proposed electrode to assess their functionality. We report ECG acquisition in wet environments and the electrode's waterproof ability, which makes them great candidates for multiple scenarios, including in sportive applications or humid environments. Another critical experiment covers the electrode's capability of self-adhesive for long-term ECG monitoring, where we report ECG signal recording for 30 minutes without using extra adhesive materials or elastic bands to fix the electrodes on the skin. Furthermore, we perform a bending experiment of up to 200 bending times to report the proposed electrodes' flexibility while maintaining its performance. Finally, we evaluated the mechanical effect of the SU-8 and PMMA/SU-8 material using the tensile test which revealed a higher toughness in the PMMA/SU-8 composite meaning higher resistance to breakage of the TPM electrodes. The multiple advantages of TPM electrodes indicate their efficiency for wearable long-term ECG monitoring in clinical-grade signal performance.

CHAPTER 7.

BIBLIOGRAPHY

[1] P. Karthikeyan, M. Murugappan, and S. Yaacob, "Detection of human stress using short-term ECG and HRV signals," *Journal of Mechanics in Medicine and Biology*, vol. 13, no. 02, p. 1350038, Apr. 2013. https://doi.org/10.1142/S0219519413500383

[2] F. Agrafioti, D. Hatzinakos, and A. K. Anderson, "ECG Pattern Analysis for Emotion Detection," *IEEE Transactions on Affective Computing*, vol. 3, no. 1, pp. 102–115, Jan. 2012. DOI: 10.1109/T-AFFC.2011.28

[3] Savonitto, Stefano, et al. "Prognostic Value of the Admission Electrocardiogram in Acute Coronary Syndromes," *JAMA*, vol. 281, no. 8, p. 707, Feb. 1999. [Online]. DOI: 10.1001/jama.281.8.707

[4] P. J. Zimetbaum and M. E. Josephson, "Use of the Electrocardiogram in Acute Myocardial Infarction," *New England Journal of Medicine*, vol. 348, no. 10, pp. 933–940, Mar. 2003. DOI: 10.1056/NEJMra022700

[5] J. W. Mason, "A Comparison of Electrophysiologic Testing with Holter Monitoring to Predict Antiarrhythmic-Drug Efficacy for Ventricular Tachyarrhythmias," *New England Journal of Medicine*, vol. 329, no. 7, pp. 445–451, Aug. 1993. DOI: 10.1056/NEJM199308123290701

[6] L. McNichol, C. Lund, T. Rosen, and M. Gray, "Medical Adhesives and Patient Safety: State of the Science Consensus Statements for the Assessment, Prevention, and Treatment of Adhesive-Related Skin Injuries," *Journal of Wound, Ostomy & Continence Nursing*, vol. 40, no. 4, pp. 365–380, Jul. 2013. DOI: 10.1097/NOR.0b013e3182a39caf

[7] N. Meziane, J. G. Webster, M. Attari, and A. J. Nimunkar, "Dry electrodes for electrocardiography," *Physiological Measurement*, vol. 34, no. 9, pp. R47–R69, Sep. 2013. DOI 10.1088/0967-3334/34/9/R47

[8] D. Huang, J. Li, T. Li, Z. Wang, Q. Wang, and Z. Li, "Recent advances on fabrication of microneedles on the flexible substrate," *Journal of Micromechanics and Microengineering*, vol. 31, no. 7, p. 073001, Jul. 2021. DOI 10.1088/1361-

6439/ac0513

[9] S. M. Lee, K. S. Sim, K. K. Kim, Y. G. Lim, and K. S. Park, “Thin and flexible active electrodes with shield for capacitive electrocardiogram measurement,” *Medical & Biological Engineering & Computing*, vol. 48, no. 5, pp. 447–457, May 2010. https://doi.org/10.1007/s11517-010-0597-y

[10] F. Stauffer, M. Thielen, C. Sauter, S. Chardonnens, S. Bachmann, K. Tybrandt, C. Peters, C. Hierold, and J. Vörös, “Skin Conformal Polymer Electrodes for Clinical ECG and EEG Recordings,” *Advanced Healthcare Materials*, vol. 7, no. 7, p. 1700994, Apr. 2018. https://doi.org/10.1002/adhm.201700994

[11] A. Gowda, B. Healey, H. Ezaldein, and M. Merati, “A Systematic Review Examining the Potential Adverse Effects of Microneedling,” The Journal of Clinical and Aesthetic Dermatology, vol. 14, no. 1, pp. 45–54, Jan. 2021. https://doi.org/10.1371/journal.pmed.1000097

[12] H. Zhang, W. Pei, Y. Chen, X. Guo, X. Wu, X. Yang, and H. Chen, “A Motion Interference-Insensitive Flexible Dry Electrode,” *IEEE Transactions on Biomedical Engineering*, vol. 63, no. 6, pp. 1136–1144, Jun. 2016. DOI: 10.1109/TBME.2015.2485269

[13] M. Matteucci, R. Carabalona, M. Casella, E. Di Fabrizio, F. Gramatica, M. Di Rienzo, E. Snidero, L. Gavioli, and M. Sancrotti, “Micropatterned dry electrodes for brain–computer interface,” *Microelectronic Engineering*, vol. 84, no. 5-8, pp. 1737–1740, May 2007. https://doi.org/10.1016/j.mee.2007.01.243

[14] M. Arai, Y. Nishinaka, and N. Miki, “Electroencephalogram measurement using polymer-based dry microneedle electrode,” *Japanese Journal of Applied Physics*, vol. 54, no. 6S1, p. 06FP14, Jun. 2015. DOI 10.7567/JJAP.54.06FP14

[15] L. Ren, S. Xu, J. Gao, Z. Lin, Z. Chen, B. Liu, L. Liang, and L. Jiang, “Fabrication of Flexible Microneedle Array Electrodes for Wearable Bio-Signal Recording,” *Sensors*, vol. 18, no. 4, p. 1191, Apr. 2018. https://doi.org/10.3390/s18041191

[16] A. K. Srivastava, B. Bhartia, K. Mukhopadhyay, and A. Sharma, “Long term biopotential recording by body conformable photolithography fabricated low cost polymeric microneedle arrays,” *Sensors and Actuators A: Physical*, vol. 236, pp. 164–172, Dec. 2015. https://doi.org/10.1016/j.sna.2015.10.041

[17] Y. Gao, V. V. Soman, J. P. Lombardi, P. P. Rajbhandari, T. P. Dhakal, D. G.

Wilson, M. D. Poliks, K. Ghose, J. N. Turner, and Z. Jin, “Heart Monitor Using Flexible Capacitive ECG Electrodes,” *IEEE Transactions on Instrumentation and Measurement*, vol. 69, no. 7, pp. 4314–4323, Jul. 2020. DOI: 10.1109/TIM.2019.2949320

[18] T.-W. Wang, H. Zhang, and S.-F. Lin, “Influence of Capacitive Coupling on High-Fidelity Non-Contact ECG Measurement,” *IEEE Sensors Journal*, vol. 20, no. 16, pp. 9265–9273, Aug. 2020. DOI: 10.1109/JSEN.2020.2986723

[19] T. Kato, A. Ueno, S. Kataoka, H. Hoshino, and Y. Ishiyama, “An Application of Capacitive Electrode for Detecting Electrocardiogram of Neonates and Infants,” in *2006 International Conference of the IEEE Engineering in Medicine and Biology Society*. New York, NY: IEEE, Aug. 2006, pp. 916–919. DOI: 10.1109/IEMBS.2006.260362

[20] A. Zompanti, A. Sabatini, S. Grasso, G. Pennazza, G. Ferri, G. Barile, M. Chello, M. Lusini, and M. Santonico, “Development and Test of a Portable ECG Device with Dry Capacitive Electrodes and Driven Right Leg Circuit,” *Sensors*, vol. 21, no. 8, p. 2777, Apr. 2021. https://doi.org/10.3390/s21082777

[21] A. Alam, A. Q. Ansari, and S. Urooj, “Design of Contactless Capacitive Electrocardiogram (ECG) Belt System,” in *2022 IEEE Delhi Section Conference (DELCON)*. New Delhi, India: IEEE, Feb. 2022, pp. 1–4. DOI: 10.1109/DELCON54057.2022.9753267

[22] J. Lee, J. Heo, W. Lee, Y. Lim, Y. Kim, and K. Park, “Flexible Capacitive Electrodes for Minimizing Motion Artifacts in Ambulatory Electrocardiograms,” *Sensors*, vol. 14, no. 8, pp. 14 732–14 743, Aug. 2014. https://doi.org/10.3390/s140814732

[23] D. U. Uguz, Z. T. Canbaz, C. H. Antink, M. Luken, and S. Leonhardt, “A Novel Sensor Design for Amplitude Modulated Measurement of Capacitive ECG,” *IEEE Transactions on Instrumentation and Measurement*, vol. 71, pp. 1–10, 2022. DOI: 10.1109/TIM.2022.3145401

[24] H. Ullah, M. A. Wahab, G. Will, M. R. Karim, T. Pan, M. Gao, D. Lai, Y. Lin, and M. H. Miraz, “Recent Advances in Stretchable and Wearable Capacitive Electrophysiological Sensors for Long-Term Health Monitoring,” *Biosensors*, vol. 12, no. 8, p. 630, Aug. 2022. https://doi.org/10.3390/bios12080630

[25] G. Li, Z. Qiu, Y. Wang, Y. Hong, Y. Wan, J. Zhang, J. Yang, Z. Wu, W. Hong,

and C. F. Guo, “PEDOT:PSS/Grafted-PDMS Electrodes for Fully Organic and Intrinsically Stretchable Skin-like Electronics,” ACS Applied Materials & Interfaces, vol. 11, no. 10, pp. 10 373–10 379, Mar. 2019. https://doi.org/10.1021/acsami.8b20255

[26] L. Zhang, K. S. Kumar, H. He, C. J. Cai, X. He, H. Gao, S. Yue, C. Li, R. C.-S. Seet, H. Ren, and J. Ouyang, “Fully organic compliant dry electrodes self-adhesive to skin for long-term motion-robust epidermal biopotential monitoring,” *Nature Communications*, vol. 11, no. 1, p. 4683, Sep. 2020. https://doi.org/10.1038/s41467-020-18503-8

[27] L. M. Ferrari, S. Sudha, S. Tarantino, R. Esposti, F. Bolzoni, P. Cavallari, C. Cipriani, I. Mattoli, and F. Greco, “Ultraconformable Temporary Tattoo Electrodes for Electrophysiology,” Advanced Science, vol. 5, no. 3, p. 1700771, Mar. 2018. https://doi.org/10.1002/advs.201700771

[28] Y. Wang, Y. Qiu, S. K. Ameri, H. Jang, Z. Dai, Y. Huang, and N. Lu, “Low-cost, m-thick, tape-free electronic tattoo sensors with minimized motion and sweat artifacts,” *npj Flexible Electronics*, vol. 2, no. 1, p. 6, Feb. 2018. https://doi.org/10.1038/s41528-017-0019-4

[29] H.-L. Peng, J.-Q. Liu, H.-C. Tian, B. Xu, Y.-Z. Dong, B. Yang, X. Chen, and C.-S. Yang, “Flexible dry electrode based on carbon nanotube/polymer hybrid micropillars for biopotential recording,” Sensors and Actuators A: Physical, vol. 235, pp. 48–56, Nov. 2015. https://doi.org/10.1016/j.sna.2015.09.024

[30] T. Kim, J. Park, J. Sohn, D. Cho, and S. Jeon, “Bioinspired, Highly Stretchable, and Conductive Dry Adhesives Based on 1D–2D Hybrid Carbon Nanocomposites for All-in-One ECG Electrodes,” *ACS Nano*, vol. 10, no. 4, pp. 4770–4778, Apr. 2016. https://doi.org/10.1021/acsnano.6b01355

[31] M. K. Yapici, T. Alkhidir, Y. A. Samad, and K. Liao, “Graphene-clad textile electrodes for electrocardiogram monitoring,” *Sensors and Actuators B: Chemical*, vol. 221, pp. 1469–1474, Dec. 2015. https://doi.org/10.1016/j.snb.2015.07.111

[32] M.-S. Cao, X.-X. Wang, W.-Q. Cao, and J. Yuan, “Ultrathin graphene: electrical properties and highly efficient electromagnetic interference shielding,” *Journal of Materials Chemistry C*, vol. 3, no. 26, pp. 6589–6599, 2015. https://doi.org/10.1039/C5TC01354B

[33] A. A. Balandin, S. Ghosh, W. Bao, I. Calizo, D. Teweldebrhan, F. Miao, and

C. N. Lau, “Superior Thermal Conductivity of Single-Layer Graphene,” *Nano Letters*, vol. 8, no. 3, pp. 902–907, Mar. 2008. https://doi.org/10.1021/nl0731872

[34] D. G. Papageorgiou, I. A. Kinloch, and R. J. Young, “Mechanical properties of graphene and graphene-based nanocomposites,” *Progress in Materials Science*, vol. 90, pp. 75–127, Oct. 2017. https://doi.org/10.1016/j.pmatsci.2017.07.004

[35] S. Kabiri Ameri, R. Ho, H. Jang, L. Tao, Y. Wang, L. Wang, D. M. Schnyer, D. Akinwande, and N. Lu, “Graphene Electronic Tattoo Sensors,” *ACS Nano*, vol. 11, no. 8, pp. 7634–7641, Aug. 2017. https://doi.org/10.1021/acsnano.7b02182

[36] Zhang, L., Kumar, K. S., He, H., Cai, C. J., He, X., Gao, H., Yue, S., Li, C., Seet, R. C.-S., Ren, H., & Ouyang, J. (2020). Fully organic compliant dry electrodes self-adhesive to skin for long-term motion-robust epidermal biopotential monitoring. Nature Communications, 11(1). https://doi.org/10.1038/s41467-020-18503-8

[37] Kim, D.-H., Lu, N., Ma, R., Kim, Y.-S., Kim, R.-H., Wang, S., Wu, J., Won, S. M., Tao, H., Islam, A., Yu, K. J., Kim, T., Chowdhury, R., Ying, M., Xu, L., Li, M., Chung, H.-J., Keum, H., McCormick, M., Rogers, J. A. (2011). Epidermal electronics. Science, 333(6044), 838–843. https://doi.org/10.1126/science.1206157

[38] Yapici, M.K. and Alkhidir, T.E., 2017. Intelligent medical garments with graphene-functionalized smart-cloth ECG sensors. Sensors, 17(4), p.875. https://doi.org/10.3390/s17040875

[39] Guler, S., Golparvar, A., Ozturk, O. and Yapici, M.K., 2022. Ear electrocardiography with soft graphene textiles for hearable applications. IEEE Sensors Letters, 6(9), pp.1-4. DOI: 10.1109/LSENS.2022.3198279

[40] Tseng, A. A., Kuan Chen, Chen, C. D., & Ma, K. J. (2003). Electron beam lithography in nanoscale fabrication: Recent development. IEEE Transactions on Electronics Packaging Manufacturing, 26(2), 141–149. https://doi.org/10.1109/tepm.2003.817714

[41] Doll, P. W., Al-Ahmad, A., Bacher, A., Muslija, A., Thelen, R., Hahn, L., Ahrens, R., Spindler, B., & Guber, A. E. (2019). Fabrication of silicon nanopillar arrays by electron beam lithography and reactive ion etching for advanced bacterial adhesion studies. Materials Research Express, 6(6), 065402. https://doi.org/10.1088/2053-1591/ab0a16

[42] Asakawa, K., & Hiraoka, T. (2002). Nanopatterning with microdomains of block copolymers using reactive-ion etching selectivity. Japanese Journal of Applied

Physics, 41(Part 1, No. 10), 6112–6118. https://doi.org/10.1143/jjap.41.6112

[43] Liu, C.-C., Nealey, P. F., Ting, Y.-H., & Wendt, A. E. (2007). Pattern transfer using poly(styrene-block-methyl methacrylate) Copolymer Films and reactive ion etching. Journal of Vacuum Science & Technology B: Microelectronics and Nanometer Structures Processing, Measurement, and Phenomena, 25(6), 1963–1968. https://doi.org/10.1116/1.2801884

[44] Klabunde, R. E. (2022). Cardiovascular Physiology Concepts. Wolters Kluwer.

[45] Webster, J. G. (1998). Medical instrumentation: Application and design. J. Wiley & Sons.

[46] Herring, N., Paterson, D. J., & Levick, J. R. (2018). Levick's introduction to Cardiovascular Physiology. CRC Press.

[47] Barold, S.S. Willem Einthoven and the Birth of Clinical Electrocardiography a Hundred Years Ago. Card Electrophysiol Rev 7, 99–104 (2003). https://doi.org/10.1023/A:1023667812925.

[48] Macfarlane, P. W. (2011). Comprehensive electrocardiology. Springer.

[49] Huszank, R., Szilágyi, E., Szoboszlai, Z., & Szikszai, Z. (2019). Investigation of chemical changes in PMMA induced by 1.6 mev he+ irradiation by ion beam analytical methods (RBS-ERDA) and infrared spectroscopy (ATR-FTIR). Nuclear Instruments and Methods in Physics Research Section B: Beam Interactions with Materials and Atoms, 450, 364–368. https://doi.org/10.1016/j.nimb.2018.05.016

[50] Singho, N. D., Lah, N. A., Johan, M. R., & Ahmad, R. (2012). Ftir Studies on silver-poly(methylmethacrylate) nanocomposites via in-situ polymerization technique. International Journal of Electrochemical Science, 7(6), 5596–5603. https://doi.org/10.1016/s1452-3981(23)19646-5

[51] Andok, R., Benčurová, A., Nemec, P., Konečníková, A., Matay, L., Škriniarová, J., & Hrkút, P. (2013). The AZ 5214e resist in EBDW lithography and its use as a Rie etch–mask in etching thin AG layers in N2 plasma. Journal of Electrical Engineering, 64(6), 371–375. https://doi.org/10.2478/jee-2013-0056

[52] Rimal, S., Koskey, S., Mukherjee, T., Goswami, A., Abdelghani, J., Ross, N. and Chyan, O., 2012, December. Interfacial characterization of post-etch polymer residues and plasma treated Cu surfaces related to advanced Cu interconnects. In Proc. SEMICON Korea.

[53] M. S. Spach, R. C. Barr, J. W. Havstad, and E. C. Long, "Skin- Electrode Impedance and Its Effect on Recording Cardiac Potentials," *Circulation*, vol. 34,

no. 4, pp. 649–656, Oct. 1966. https://doi.org/10.1161/01.CIR.34.4.649

[54] Izadi, H. and Penlidis, A. (2013), Polymeric Bio-Inspired Dry Adhesives: Van der Waals or Electrostatic Interactions?. Macromol. React. Eng., 7: 588-608. https://doi.org/10.1002/mren.201300146

[55] S. Chun, D. W. Kim, S. Baik, H. J. Lee, J. H. Lee, S. H. Bhang, and C. Pang, "Conductive and Stretchable Adhesive Electronics with Miniaturized Octopus-Like Suckers against Dry/Wet Skin for Biosignal Monitoring," *Advanced Functional Materials*, vol. 28, no. 52, p. 1805224, Dec. 2018. https://doi.org/10.1002/adfm.201805224

[56] Abbas, T.M. and Hussein, S.I., 2022. Improving the mechanical properties, roughness, thermal stability, and contact angle of the acrylic polymer by graphene and carbon fiber doping for waterproof coatings. Journal of Inorganic and Organometallic Polymers and Materials, 32(10), pp.3788-3796. https://doi.org/10.1007/s10904-022-02384-z

[57] Yu, H., Balogun, O., Li, B., Murray, T. W., & Zhang, X. (2004). Building embedded microchannels using a single layered su-8, and determining Young's modulus using a laser acoustic technique. Journal of Micromechanics and Microengineering, 14(11), 1576–1584. https://doi.org/10.1088/0960-1317/14/11/020

[58] Chung, S., & Park, S. (2013). Effects of temperature on mechanical properties of SU-8 photoresist material. Journal of Mechanical Science and Technology, 27(9), 2701–2707. https://doi.org/10.1007/s12206-013-0714-6

[59] Ritchie, R. O. (2011). The conflicts between strength and toughness. Nature Materials, 10(11), 817–822. https://doi.org/10.1038/nmat3115